

Soft Matter

Accepted Manuscript



This is an *Accepted Manuscript*, which has been through the Royal Society of Chemistry peer review process and has been accepted for publication.

Accepted Manuscripts are published online shortly after acceptance, before technical editing, formatting and proof reading. Using this free service, authors can make their results available to the community, in citable form, before we publish the edited article. We will replace this *Accepted Manuscript* with the edited and formatted *Advance Article* as soon as it is available.

You can find more information about *Accepted Manuscripts* in the [Information for Authors](#).

Please note that technical editing may introduce minor changes to the text and/or graphics, which may alter content. The journal's standard [Terms & Conditions](#) and the [Ethical guidelines](#) still apply. In no event shall the Royal Society of Chemistry be held responsible for any errors or omissions in this *Accepted Manuscript* or any consequences arising from the use of any information it contains.

Capillary Instability of Axisymmetric, Active Liquid Crystal Jets

Xiaogang Yang* and Qi Wang†

Abstract

We study linear stability of an infinitely long, axisymmetric, cylindrical *active liquid crystal (ALC) jet* in a passive isotropic fluid matrix using a polar active liquid crystal (ALC) model. We identify three possible unstable modes (or mechanisms) as the result of the interaction between the flow and the active (or self-propelled) molecular motion. The first unstable mode is related to the *polarity vector instability* when coupled to the flow field at the presence of the molecular activity. It can be traced back to the inherent polarity vector instability in a bulk active liquid crystal flow. However, it can be grossly amplified in the ALC jet to encompass up to infinitely many unstable growth rates when the long range distortional elastic interaction is weak in certain parameter regimes; it can also be suppressed in other parameter regimes completely. The second unstable mode is related to the classical capillary or Rayleigh instability, which exists in a finite wave interval $[0, k_{cutoff}]$. The new feature for this instability lies in the dependence of the cutoff wave number (k_{cutoff}) on the activity of the active matter system. For ALC jets with sufficiently strong contractile activity, the instability can be completely suppressed though. The third unstable mode is due to the active viscous stress. This unstable mode can emerge in the intermediate wave number regime at a sufficiently strong active viscosity and even expand all the way to the zero wave number limit when the Rayleigh unstable mode is absent. It can also be suppressed in the regime of weak active viscous stress. At any given values of the model parameters, the three types of instabilities can show up either individually or in a certain combination, or be completely suppressed altogether. In this paper, we discuss the positive growth rates associated with the instabilities, the windows of instability and their dependence on model parameters through extensive numerical computations aided by asymptotic analysis.

1 Introduction

Active matter refers to the materials that are driven out of equilibrium by energy input at the microscopic scale via biological or catalytic activities. As a consequence, some emergent dynamical structures may result in the material systems, such as long-range order, anomalous fluctuations, spontaneous flows, dynamical spatial-temporal structures and patterns [1, 2, 3, 4, 5, 6, 7, 8, 9, 10,

*nkyxg@mail.nankai.edu.cn, School of Mathematical Sciences, Nankai University, Tianjin, China 300071

†qwang@math.sc.edu, Department of Mathematics, Interdisciplinary Mathematics Institute and NanoCenter at USC University of South Carolina, Columbia, SC 29028; School of Mathematical Sciences, Nankai University, Tianjin, China 300071; Beijing Computational Science Research Center, Beijing, China 100084

11]. When coupled with regulatory signaling pathways, active materials can serve as models for living systems such as cortical layers in the cytoskeleton of cells and bacterial colonies in bacterial biofilms [12, 13, 14, 15, 16].

Active particles in the active matter are generally anisotropic in their configuration and motion, and can form self-assembled ordered states with respect to orientation [17, 18]. The nature of the ordered state depends on both the configuration of the individual particle and the interaction among the particles. A class of active materials with these features is the active liquid crystal, which may form liquid crystalline phases at a sufficiently high particle concentration or under sufficiently strong particle-particle interactions [19, 20]. When the particle immersed in a solution possesses a distinctive head and tail, the particle-fluid system is called a polar active liquid crystal solution. Examples in this class of materials include bacterial suspensions, asymmetric vibrated granular rods, polarized migrating cells, and catalytic charged nano-particles in a solution. Self-propelled particles are often modeled as polar active particles, where the activity is incorporated via a self-propelled velocity of the individual particle. The interaction between the self-propelled particle and the host fluid matrix is characterized by an active bulk stress and, in some cases, an additional active viscous stress. When the active particle demonstrates a head-tail symmetry in its configuration, the active liquid crystal system is called an apolar liquid crystal system, which includes vibrated rods. We note that this system is also referred to as the shaker in some literature, where nematic steric interaction may be more prominent [21, 22]. The nature of the particle-particle interaction is crucial in determining properties of the ordered state. Polar particles may experience either polar interaction, i.e., the one that tends to orient particles head to head and tail to tail, or interactions that are apolar, i.e., those that orient particles regardless of their polarity, or both [23, 24].

The polar active liquid crystal can order in polar states, described by a nonzero vector order parameter and mean motion. The vector order parameter is often referred to as the polarity vector or polar order parameter, whose orientation and magnitude measures the direction and strength of polarity, respectively. Apolar active particles generally experience apolar interactions and the resulting ordered state exhibits the symmetry of nematic liquid crystals. A vector order parameter that is invariant with respect to the head-tail reflection, or a second order tensor order parameter, can be employed to describe the broken symmetry [19, 24]. There exists a class of active liquid crystals that exhibits nematic symmetry at large scales due to the apolar steric interaction and hydrodynamic coupling, but consists of self-propelled particles (hence it is polar at the micro scale.) Such a system includes swimmers in a bulk suspension [25, 26]. These interactions lead to large-scale nematics with weak or no polar order [27, 28]. For this class of active liquid crystals, a vector order parameter along with a tensor order parameter form the minimal set of order parameters to describe its broken symmetry [18]. In the real world, this class of active liquid crystals includes gliding myxobacteria, suspensions of auto-catalytic Janus colloids and motile epithelial cells [29, 30]. It therefore represents an important class of active matter systems of direct physical relevance.

A useful theoretical framework for describing the collective behavior of active matter systems is the continuum model that extends liquid crystal hydrodynamics to include new activities due to the microscopic energy input [19]. For polar active liquid crystals, minimal continuum models use a single vector to describe the broken symmetry [17, 31, 18]. For apolar active liquid crystals, either a single vector with the reflective symmetry enforced or a second order tensor with the built-in reflective symmetry can be employed to describe the molecular orientation. For more

general active liquid crystals whose active particles are primarily polar while the interactions may be dominated by apolar interactions, both a single vector and a second order tensor order parameter are required to describe the broken symmetry [24]. In these continuum models, sources of coarse-grain molecular activities are implemented as low order perturbations to the corresponding passive liquid crystal systems [16, 19, 13, 32, 18]. A more detailed theoretical description of active liquid crystals is the phase space or configurational space kinetic theory pioneered by Marchetti and Liverpool and Shelley *et al.*, and extended by Forest *et al.* [18, 33, 34, 35, 35, 36, 37, 38, 39]. In this formulation of models for active liquid crystals, microscopic scale symmetry is tacitly incorporated through the interaction potential, self-propelled velocity, as well as phenomenological active forces [40]. This formulation can unify all three types of continuum models by paying careful attention to closure procedures. For detailed reviews on the mathematical models for active matter systems, please refer to some recent excellent review papers on this topic by a group of leading experts in this field [17, 18].

Emergent spatial-temporal structures in active liquid crystals are predominantly driven by instabilities [33, 41, 42]. These instabilities can sustain macroscopic global structures in time and space as well as transient defective structures [43, 44, 13], making the active liquid crystal a very interesting material system to study for the interaction between hydrodynamics and molecular driven activities. In reality, many active matter systems are exposed in domains where the boundary between the active material system and the ambient deformable materials is free, forming a free surface dynamical initial-boundary value problem. For instance, when a liquid filament of active materials is suspended in an ambient liquid matrix, the interface between the active material and the host matrix is going to be determined by the property of the active material and the host matrix together with their interactions at the free interface. In this paper, we will focus on one of such problems to investigate how active material's properties can alter the interfacial instability of a polar ALC filament or jet, also known as the capillary instability, to contrast the contribution of the active material's activity to classical interfacial hydrodynamics.

Capillary instability of (passive) liquid crystal jets has been studied by several groups in the past [45, 46, 47, 48, 42, 49, 41, 50]. Bulk elasticity, molecular anisotropy, anchoring condition, and long-range elasticity have been shown to be able to impact the classical Rayleigh capillary instability by shifting the cut-off wave number and lowering the growth rate so as to "stabilize" the jet [45, 46, 47, 48, 50]. With an long-range elastic effect at the free surface considered, Fel and Zimmels reported an additional elastic instability in long waves in the elastic regime [50]. In this paper, we extend the studies to investigate how internally generated molecular activities can affect stability of the ALC jet.

We extend a minimal polar active liquid crystal model developed by Marchetti *et al.* [44, 18] and couple it to a passive isotropic fluid matrix in a free surface problem. We then use it to investigate how a liquid filament or jet of active liquid crystals when suspended in an isotropic liquid matrix can alter the classical Rayleigh instability and moreover to induce additional instabilities that are related to inherent instability in the active liquid crystal system in certain parameter regimes. In an infinitely long, isotropic liquid jet, the classical capillary instability occurs in the wavelength range that is confined by the radius of the liquid jet. When the molecular activity is taken into account in the active liquid crystal model, the scenario can be modified in such a way that certain molecular activities can promote the instability while others suppress it, making the active liquid crystal an ideal candidate for enhanced material processing. In this study, we will also explore the role of the so-called active viscous stress on stability of the free surface liquid jet. Active liquid

crystal flows are inherently unstable with and without a boundary, in which spontaneous flows can ensue at sufficiently strong activity or the presence of boundaries [32, 51, 52, 53, 54, 55, 56]. In the problem we are going to study, we neglect the weak elastic surface force due to the long range molecular interaction to highlight the role of molecular activities in the active liquid crystal jet [47, 48, 50]. We also limit to essentially one type steady state jet profile in this study so that some of the inherent instabilities within the active liquid crystal system may be suppressed such as inhomogeneous patterns within the jet cross-section and the steady state in the radial direction, etc. [51, 52, 53, 54, 55, 56]. Results on stability of these steady states deserves another comprehensive investigation and therefore will not be included in this study.

The rest of the paper is organized into three sections. Firstly, we will present the minimal polar liquid crystal model coupled with a class of free surface boundary conditions suitable to the underlying free surface problem. Then, we study the linearized stability property of a class of steady state active liquid crystal jet flows subject to a class of free surface boundary conditions, in which we explore the mechanisms leading to jet stabilities and instabilities. Combining both asymptotic analysis and numerical computations, we map out the instabilities of the liquid jet flow and link them to three active mechanisms in the model. Finally, we conclude the study in the last section.

2 Mathematical Formulation for Free Surface Active Liquid Crystal Jets

We consider an axisymmetric liquid jet consisting of active liquid crystals in a passive fluid matrix or ambient fluid. For the active liquid crystal, we adopt a polar active liquid crystal solution model developed recently [44, 18]. We assume that the molecular orientation represented by the polarity orientation in the active liquid crystal solution is described by the vector polarization field \mathbf{p} also known as the polarity vector. Swimming rodlike virus has a polarity vector defined by its self-propelled moving direction and speed; live bacteria show some directional preference during their migration. For active liquid crystal systems, the polarity vector is commonly used to describe the motion as well as orientation of active molecules or active micro-particles.

We denote the free energy of the material's system by $F = F[\mathbf{p}, \nabla\mathbf{p}] = \int_V f(\mathbf{p}, \nabla\mathbf{p}) d\mathbf{x}$, where V is the material volume, f is the bulk free energy density (unit energy per unit volume). The molecular field, conjugate to the polarity vector \mathbf{p} is given by $\mathbf{h} = -\frac{\delta F}{\delta \mathbf{p}}$. We denote the mass average velocity field of the active liquid crystal solution by \mathbf{v} . With respect to this velocity field, the strain rate tensor is denoted by $\mathbf{D} = \frac{1}{2}(\nabla\mathbf{v} + \nabla\mathbf{v}^T)$ and the vorticity tensor by $\mathbf{\Omega} = \frac{1}{2}(\nabla\mathbf{v} - \nabla\mathbf{v}^T)$, where we denote $(\nabla\mathbf{v})_{\alpha\beta} = \partial_\alpha v_\beta$. Often, the active liquid crystal system is assumed to be driven out of equilibrium by a constant chemical potential difference $\Delta\mu$ between ATP and its hydrolysis products [15, 13, 14, 57].

2.1 Governing system of equations

The hydrodynamic equations for incompressible polar active liquid crystals are summarized as follows [15, 58]:

$$\begin{aligned}\frac{\partial \mathbf{p}}{\partial t} + (\mathbf{v} + w\mathbf{p}) \cdot \nabla \mathbf{p} + \Omega \cdot \mathbf{p} &= \frac{1}{\gamma} \mathbf{h} + \lambda \Delta \mu \mathbf{p} + \nu \mathbf{D} \cdot \mathbf{p}, \\ \frac{\partial(\rho \mathbf{v})}{\partial t} + \nabla \cdot (\rho \mathbf{v} \mathbf{v}) &= \nabla \cdot \boldsymbol{\sigma}, \\ \nabla \cdot \mathbf{v} &= 0,\end{aligned}\tag{2.1}$$

where ρ is the material density, ν is a geometric parameter for active liquid crystal molecules (also known as the tumbling parameter in the Ericksen-Leslie theory [59]) and the stress tensor $\boldsymbol{\sigma}$ is consisted of hydrostatic pressure (Π), reactive stress ($\boldsymbol{\sigma}^r$), dissipative stress ($\boldsymbol{\sigma}^d$), active stress ($\boldsymbol{\sigma}^a$), and Ericksen stress ($\boldsymbol{\sigma}^e$), respectively,

$$\begin{aligned}\boldsymbol{\sigma} &= \boldsymbol{\sigma}^r + \boldsymbol{\sigma}^d + \boldsymbol{\sigma}^a + \boldsymbol{\sigma}^e - \Pi \mathbf{I}, \\ \boldsymbol{\sigma}^r &= -\frac{\nu}{2}(\mathbf{p}\mathbf{h} + \mathbf{h}\mathbf{p}) + \frac{1}{2}(\mathbf{p}\mathbf{h} - \mathbf{h}\mathbf{p}), \\ \boldsymbol{\sigma}^d &= 2\eta \mathbf{D}, \\ \boldsymbol{\sigma}^a &= \beta(\nabla \mathbf{p} + \nabla \mathbf{p}^T) + \zeta \Delta \mu \mathbf{p}\mathbf{p}, \\ \boldsymbol{\sigma}^e &= f\mathbf{I} - K(\nabla \mathbf{p}) \cdot (\nabla \mathbf{p}^T), \\ \nabla \cdot \boldsymbol{\sigma}^e &= -(\nabla \mathbf{p}) \cdot \mathbf{h}.\end{aligned}\tag{2.2}$$

The active stress is consisted of two parts: the active (bulk) stress ($\zeta \mathbf{p}\mathbf{p}$) and the active viscous stress ($\beta(\nabla \mathbf{p} + \nabla \mathbf{p}^T)$) in which β is the generalized active viscosity [58]; η is the viscosity of the solution matrix; $w\mathbf{p}$ is the self-moving (self-propelling) velocity of the polar liquid crystal molecule (or particle) [58]; an additional active molecular contribution to the polarity vector is proportional to $\Delta \mu$ and characterized by coefficient λ [32, 14, 58]. We remark that the reactive stress is derived using a virtual work principle from the system's free energy [14, 15], the Ericksen stress is derived from the same variational principle associated to the elastic body force [14, 60], and the active stress is derived separately from an argument on force couples acting on the active particle. The viscous stress can be derived from a prescribed dissipation functional via variation with respect to the rate of strain tensor [61].

The molecular field, calculated from the free energy density, can be rewritten into the following using the transport equation for the polarity vector:

$$\mathbf{h} = -\frac{\delta F}{\delta \mathbf{p}} = h_1 \mathbf{p} - h_2 \|\mathbf{p}\|^2 \mathbf{p} + K \nabla^2 \mathbf{p} = \gamma \dot{\mathbf{p}} + \gamma w \mathbf{p} \cdot \nabla \mathbf{p} - \gamma \lambda \Delta \mu \mathbf{p} - \gamma \nu \mathbf{D} \cdot \mathbf{p},\tag{2.3}$$

where the free energy of the system is given by [62, 63]

$$F = \int_V \left\{ \frac{K}{2} \|\nabla \mathbf{p}\|^2 - \frac{h_1}{2} \|\mathbf{p}\|^2 + \frac{h_2}{4} \|\mathbf{p}\|^4 \right\} d\mathbf{x},\tag{2.4}$$

and $\dot{\mathbf{p}} = \frac{\partial \mathbf{p}}{\partial t} + \mathbf{v} \cdot \nabla \mathbf{p} + \boldsymbol{\Omega} \cdot \mathbf{p}$ is the convected co-rotational derivative, a frame-invariant derivative, for the polarity vector, K is the analog of the Frank elastic constant of the Ericksen-Leslie theory for liquid crystals, h_1 and h_2 are two constants parameterizing the strength of the bulk free energy. In this free energy, a one-constant approximation for the Frank elastic constant is adopted [20].

2.2 Interfacial boundary conditions

The governing equations given above are valid within the region of active liquid crystals. At the boundaries between the active liquid crystal solution and the ambient isotropic fluid, appropriate boundary conditions must be supplied. The force balance boundary condition at the free surface between the ALC and the passive fluid matrix is given by the kinetic boundary condition [64]

$$(\boldsymbol{\sigma} + \Pi_a \mathbf{I}) \cdot \mathbf{n} = \mathbf{I}_s \cdot \nabla \cdot \boldsymbol{\tau}_s = -\tau \boldsymbol{\kappa} \mathbf{n}, \quad (2.5)$$

where Π_a is the ambient fluid pressure, \mathbf{n} is the unit external normal of the jet free surface, $\boldsymbol{\tau}_s = \tau \mathbf{I}_s$ is the surface stress tensor, τ is the surface tension coefficient which is assumed a constant in this study, $\mathbf{I}_s = (\mathbf{I} - \mathbf{n}\mathbf{n})$ is the surface identity matrix, and $\boldsymbol{\kappa}$ is the mean curvature of the interfacial surface. We remark that we neglect the contribution from the elastic surface energy between the active liquid crystal and the ambient isotropic fluid in this study to highlight the role played by the activity of the ALC system [47, 48, 45, 50]. The impact of this elastic surface energy to the capillary instability will be investigated in a sequel.

To describe the motion of the free surface, we need a kinematic boundary condition. We denote the free surface by $0 = \Phi(r, \theta, z, t) = r - \phi(z, t)$ in the cylindrical coordinate system (r, θ, z) . The kinematic boundary condition is then given by

$$\left(\frac{\partial}{\partial t} + \mathbf{v} \cdot \nabla \right) \Phi = 0. \quad (2.6)$$

In this study, we focus on the axisymmetric and torsionless velocity field [64]. When the velocity field is an axisymmetric, torsionless flow field, the kinematic boundary condition reduces to

$$\frac{\partial \phi(z, t)}{\partial t} + v_z \frac{\partial \phi(z, t)}{\partial z} - v_r = 0. \quad (2.7)$$

This condition indicates that the free surface convects with the fluid flow, where $\mathbf{v} = (v_r, 0, v_z)$ represents the torsionless velocity field in the cylindrical coordinate.

In addition to these boundary conditions, the polarity vector needs boundary conditions at the free surface as well. The boundary condition for the polarity vector is tricky for active material systems since it depends on how the active molecule interact with the ambient fluid. To derive the boundary condition, we introduce a surface free energy. We denote the surface free energy by $F_s = F_s(\mathbf{p}) = \int_{\partial V} f_s(\mathbf{p}) d\mathbf{A}$, where ∂V is the surface of the active material volume, $f_s(\mathbf{p})$ is the surface free energy density (unit energy per unit area). We specify $f_s(\mathbf{p})$ as follows, based on the anchoring effect of the active liquid crystal at the free surface,

$$f_s(\mathbf{p}) = \frac{\alpha_1}{2} \|\mathbf{p} - \|\mathbf{p}\|\mathbf{t}\|^2 + \frac{\alpha_2}{2} \|\mathbf{p} - \|\mathbf{p}\|\mathbf{n}\|^2, \quad (2.8)$$

where \mathbf{n} is the unit normal vector and \mathbf{t} is the unit tangential vector normal to the polar direction \mathbf{e}_θ in the cylindrical coordinate for the axisymmetric liquid jet. If $\alpha_1 \neq 0, \alpha_2 = 0$, the surface free

energy is zero when \mathbf{p} is parallel to \mathbf{t} , that means the direction of \mathbf{p} is on the tangential plan at the free surface in the (r, z) plane. If $\alpha_1 = 0, \alpha_2 \neq 0$, the surface free energy is zero when \mathbf{p} is parallel to \mathbf{n} , that means the direction of \mathbf{p} is normal to the free surface. In this paper, we limit to the case of $\alpha_1 > 0, \alpha_2 = 0$ so that the polarity vector aligns tangentially at the minimum of the surface anchoring energy. The total free energy of the system is then given by $F^{tot} = F + F_s$, we calculate the variation $\frac{\delta F^{tot}}{\delta \mathbf{p}}$. In order to arrive at the reactive elastic stress, we need to assign the contributions from the boundary integrals in the variation into zero. This yields the boundary condition for the polarity vector at the free surface:

$$K(\nabla \mathbf{p}) \cdot \mathbf{n} + \alpha_1(2\mathbf{p} - \|\mathbf{p}\|\mathbf{t} - \frac{\mathbf{p} \cdot \mathbf{t}}{\|\mathbf{p}\|}\mathbf{p}) = 0. \quad (2.9)$$

We set $\delta = \frac{K}{\alpha_1}$, then the boundary condition can be rewritten into

$$\frac{\partial \mathbf{p}}{\partial \mathbf{n}} + \frac{1}{\delta}(2\mathbf{p} - \|\mathbf{p}\|\mathbf{t} - \frac{\mathbf{p} \cdot \mathbf{t}}{\|\mathbf{p}\|}\mathbf{p}) = 0. \quad (2.10)$$

We call this boundary condition the weak (soft) anchoring boundary condition. In the limit of $\delta \rightarrow 0$, the boundary condition reduces to $2\mathbf{p} - \|\mathbf{p}\|\mathbf{t} - \frac{\mathbf{p} \cdot \mathbf{t}}{\|\mathbf{p}\|}\mathbf{p} = 0$. It's readily shown that

$$\mathbf{p} = \|\mathbf{p}\|\mathbf{t} \quad (2.11)$$

satisfies this condition, which is called the strong anchoring condition. In the limit of $\delta \rightarrow \infty$, the boundary condition reduces to

$$\frac{\partial \mathbf{p}}{\partial \mathbf{n}} = 0, \quad (2.12)$$

this is the Neumann boundary condition, also known as the free boundary condition. In this paper, we will examine how the linear stability of the ALC jet corresponds to the boundary conditions with $\delta \in [0, \infty)$.

2.3 Dimensionless equations

The polarity vector \mathbf{p} is dimensionless and is used in this model to measure the strength and direction of polarity. We use a characteristic time scale t_0 , length scale l_0 , "strength of polarity p_L ", and mass density scale $\rho_0 = \rho$ to non-dimensionalize the physical variables and equations:

$$\tilde{t} = \frac{t}{t_0}, \quad \tilde{\mathbf{x}} = \frac{\mathbf{x}}{l_0}, \quad \tilde{\mathbf{v}} = \frac{\mathbf{v}t_0}{l_0}, \quad \tilde{\Pi} = \frac{\Pi t_0^2}{\rho_0 l_0^2}, \quad \tilde{\mathbf{h}} = \frac{\mathbf{h} t_0^2 p_L}{\rho_0 l_0^2}, \quad \tilde{\mathbf{p}} = \frac{\mathbf{p}}{p_L}.$$

Then, we obtain the following dimensionless group

$$\tilde{w} = \frac{t_0 p_L}{l_0} w, \quad \tilde{\gamma} = \frac{t_0 p_L^2}{\rho_0 l_0^2} \gamma, \quad \tilde{\lambda} = t_0 \lambda \Delta \mu, \quad \tilde{\mathbf{v}} = \mathbf{v}, \quad \tilde{h}_1 = \frac{t_0^2 p_L^2}{\rho_0 l_0^2} h_1, \quad \tilde{h}_2 = \frac{t_0^2 p_L^4}{\rho_0 l_0^2} h_2,$$

$$\tilde{K} = \frac{t_0^2 p_L^2}{\rho_0 l_0^4} K, \quad \frac{1}{\tilde{\eta}} = Re = \frac{\rho_0 l_0^2}{\eta t_0}, \quad \tilde{\beta} = \frac{t_0^2 p_L}{\rho_0 l_0^3} \beta, \quad \tilde{\zeta} = \frac{t_0^2 p_L^2}{\rho_0 l_0^2} \zeta \Delta \mu, \quad \tilde{\delta} = \frac{\delta}{l_0}, \quad \tilde{\tau} = \frac{\tau_0^2}{\rho_0 l_0^3}.$$

where Re is the Reynolds number for the solvent in the ALC system, and K is proportional to the reciprocal of the Ericksen number. We choose l_0 as the radius of the cylindrical jet and an appropriate p_L to ensure $\tilde{\gamma}\tilde{\lambda} + \tilde{h}_1 = \tilde{h}_2$ (that is $p_L^2 = \frac{\gamma\lambda + h_1}{h_2}$). Then, the dimensionless equation yields a constant solution $\tilde{\mathbf{p}} = \mathbf{p}_0, \tilde{\mathbf{v}} = \mathbf{0}$, where $\|\mathbf{p}_0\| = 1$.

For simplicity, we drop the $\tilde{}$ on the dimensionless variables and parameters. The system of governing equations for the ALC system in the dimensionless form is summarized as follows

$$\begin{aligned}
\frac{\partial \mathbf{p}}{\partial t} + (\mathbf{v} + w\mathbf{p}) \cdot \nabla \mathbf{p} + \boldsymbol{\Omega} \cdot \mathbf{p} &= \frac{1}{\gamma} \mathbf{h} + \lambda \mathbf{p} + \nu \mathbf{D} \cdot \mathbf{p}, \\
\frac{\partial \mathbf{v}}{\partial t} + \nabla \cdot (\mathbf{v}\mathbf{v}) &= \nabla \cdot \boldsymbol{\sigma}, \\
\nabla \cdot \mathbf{v} &= 0, \\
\boldsymbol{\sigma} &= -\Pi \mathbf{I} + \boldsymbol{\sigma}^e + \frac{2}{Re} \mathbf{D} + \beta (\nabla \mathbf{p} + \nabla \mathbf{p}^T) + \zeta \mathbf{p}\mathbf{p} - \frac{\nu}{2} (\mathbf{p}\mathbf{h} + \mathbf{h}\mathbf{p}) + \frac{1}{2} (\mathbf{p}\mathbf{h} - \mathbf{h}\mathbf{p}), \\
\nabla \cdot \boldsymbol{\sigma}^e &= -(\nabla \mathbf{p}) \cdot \mathbf{h}, \\
\mathbf{h} &= h_1 \mathbf{p} - h_2 \|\mathbf{p}\|^2 \mathbf{p} + K \nabla^2 \mathbf{p}.
\end{aligned} \tag{2.13}$$

The dimensionless interfacial boundary conditions are given by

$$\begin{aligned}
\frac{\partial \phi(z,t)}{\partial t} + v_z \frac{\partial \phi(z,t)}{\partial z} - \nu_r &= 0, \\
(\boldsymbol{\sigma} + \Pi_a \mathbf{I}) \cdot \mathbf{n} &= -\tau \kappa \mathbf{n}, \\
\frac{\partial \mathbf{p}}{\partial \mathbf{n}} + \frac{1}{\delta} (2\mathbf{p} - \|\mathbf{p}\| \mathbf{t} - \frac{\mathbf{p} \cdot \mathbf{t}}{\|\mathbf{p}\|} \mathbf{p}) &= 0.
\end{aligned} \tag{2.14}$$

We denote $\bar{h}_1 = h_1 + \gamma\lambda$ and $\mathbf{h}_e = \mathbf{h} + \gamma\lambda \mathbf{p} = \bar{h}_1 \mathbf{p} - h_2 \|\mathbf{p}\|^2 \mathbf{p} + K \nabla^2 \mathbf{p}$. Then, we have

$$\begin{aligned}
\mathbf{p}\mathbf{h} - \mathbf{h}\mathbf{p} &= \mathbf{p}\mathbf{h}_e - \mathbf{h}_e \mathbf{p}, \quad \mathbf{p}\mathbf{h} + \mathbf{h}\mathbf{p} = \mathbf{p}\mathbf{h}_e + \mathbf{h}_e \mathbf{p} - 2\gamma\lambda \mathbf{p}\mathbf{p}, \\
\nabla \cdot \boldsymbol{\sigma}^e &= -(\nabla \mathbf{p}) \cdot \mathbf{h} = -(\nabla \mathbf{p}) \cdot \mathbf{h}_e + \frac{1}{2} \gamma \lambda \nabla \cdot (\|\mathbf{p}\|^2 \mathbf{I}).
\end{aligned} \tag{2.15}$$

Notice that active parameter λ also gives a contribution to the active stress in $\gamma\lambda \nu \mathbf{p}\mathbf{p}$ as well as a contribution to the pressure $\frac{1}{2} \gamma \lambda \nabla \cdot (\|\mathbf{p}\|^2 \mathbf{I})$, which can be absorbed into the pressure term $-\Pi \mathbf{I}$. Let $\bar{\zeta} = \zeta + \gamma\lambda \nu$, $\bar{\Pi} = \Pi - \frac{1}{2} \gamma \lambda \|\mathbf{p}\|^2$, we can eliminate parameter λ if we use $\bar{h}_1, \mathbf{h}_e, \bar{\zeta}, \bar{\Pi}$ instead of $h_1, \mathbf{h}, \zeta, \Pi$ respectively. So we can further assume $\lambda = 0$ and $h_1 = \bar{h}_1 = h_2$ in the dimensionless equation system from now on. This simplification is equivalent to adding a harmonic potential, due to the molecular activity associated with the polarity vector, to the equilibrium free energy, demonstrating another source of active stress in the polar active liquid crystal system.

In the following, we examine linear stability properties of a simple steady state of constant radius and velocity of the governing system of equations subject to the interfacial boundary conditions, through which we can investigate the near equilibrium dynamics of the free surface active liquid crystal jet.

3 Linear Stability Analysis

It is easy to show that $\phi = 1$, $\mathbf{v} = \mathbf{v}_0$, $\mathbf{p} = \mathbf{p}_0 = (0, 0, 1)$, $\Pi = \Pi_0$ is a steady state solution for all the anchoring boundary conditions with $\delta \in [0, \infty)$, where \mathbf{v}_0 is a constant vector and Π_0 is a constant pressure determined by the equilibrium force balance at the interface: $\Pi_a - \Pi_0 + \tau\kappa = 0$. Without loss of generality, we set the constant velocity $\mathbf{v}_0 = \mathbf{0}$, then, the jet is also known as a liquid filament. In this section, we investigate linear stability of the constant equilibrium state of the jet or the filament, often referred to as the capillary instability or Rayleigh instability analysis [64, 48, 47, 49, 42, 65]. We linearize the governing system of equations (including the boundary conditions) around the steady state and seek solutions of the following form

$$\phi = 1 + \varepsilon e^{\alpha r + ikz} \phi_1, \quad \mathbf{v} = \varepsilon e^{\alpha r + ikz} \mathbf{v}_1(r), \quad \mathbf{p} = \mathbf{p}_0 + \varepsilon e^{\alpha r + ikz} \mathbf{p}_1(r), \quad \Pi = \Pi_0 + \varepsilon e^{\alpha r + ikz} \Pi_1(r), \quad (3.1)$$

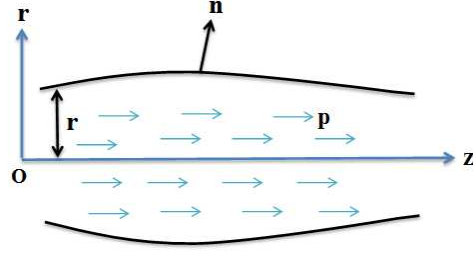
where ϕ_1 is a constant unknown, and $\mathbf{v}_1(r)$, $\mathbf{p}_1(r)$, $\Pi_1(r)$ are variable unknowns (which are functions of r) to be determined by the linearized equations together with the linearized boundary conditions.

For the torsionless mode [64], the linearization of the governing equations together with the boundary conditions yields the following linear ordinary differential equations,

$$\begin{aligned} \alpha p_{1r} + ikwp_{1r} &= \frac{1}{\gamma}(K(p''_{1r} + \frac{1}{r}p'_{1r} - \frac{1}{r^2}p_{1r}) - k^2Kp_{1r}) + \frac{\nu-1}{2}v'_{1z} + ik\frac{\nu+1}{2}v_{1r}, \\ \alpha p_{1z} + ikwp_{1z} &= \frac{1}{\gamma}(-2h_2p_{1z} + K(p''_{1z} + \frac{1}{r}p'_{1z}) - k^2Kp_{1z}) + ikvv_{1z}, \\ \alpha v_{1r} &= -\Pi'_1 + \eta(v''_{1r} + \frac{1}{r}v'_{1r} - \frac{1}{r^2}v_{1r} - k^2v_{1r}) + 2\beta(p''_{1r} + \frac{1}{r}p'_{1r} - \frac{1}{r^2}p_{1r}) + \\ &\beta(ikp'_{1z} - k^2p_{1r}) + (\nabla \cdot \boldsymbol{\sigma}^p)_r^0, \\ \alpha v_{1z} &= -ik\Pi_1 + \eta(v''_{1z} + \frac{1}{r}v'_{1z} - k^2v_{1z}) - 2\beta k^2p_{1z} + \beta(p''_{1z} + \frac{1}{r}p'_{1z} + \\ &ikp'_{1r} + \frac{ik}{r}p_{1r}) + (\nabla \cdot \boldsymbol{\sigma}^p)_z^0, \\ v'_{1r}(r) + \frac{v_{1r}(r)}{r} + ikv_{1z}(r) &= 0, \end{aligned} \quad (3.2)$$

where

$$\begin{aligned} (\nabla \cdot \boldsymbol{\sigma}^p)_r^0 &= \zeta(ikp_{1r}) - \frac{\gamma}{2}(\nu + 1)(ik\alpha p_{1r} + \frac{ik}{2}(-ikv_{1r} + v'_{1z})) \\ &+ \frac{\nu\gamma}{2}(\nu + 1)(\frac{ik}{2}(ikv_{1r} + v'_{1z})) - \frac{w\gamma}{2}(\nu + 1)(-k^2p_{1r}), \\ (\nabla \cdot \boldsymbol{\sigma}^p)_z^0 &= \zeta(\frac{1}{r}p_{1r} + p'_{1r} + 2ikp_{1z}) - \frac{\gamma}{2}(\nu + 1)(ik\alpha p_{1z}) \\ &- \frac{\gamma}{2}(\nu - 1)(\alpha(\frac{1}{r}p_{1r} + p'_{1r} + ikp_{1z}) + \frac{1}{2}(\frac{1}{r}(-ikv_{1r} + v'_{1z}) - ikv'_{1r} + v''_{1z})) \\ &+ \frac{\nu\gamma}{2}(\nu + 1)(-k^2v_{1z}) + \frac{\nu\gamma}{2}(\nu - 1)(\frac{1}{2}(\frac{1}{r}(ikv_{1r} + v'_{1z}) + ikv'_{1r} + v''_{1z}) - k^2v_{1z}) \\ &- \frac{w\gamma}{2}(\nu + 1)(-k^2p_{1z}) - \frac{w\gamma}{2}(\nu - 1)(\frac{ik}{r}p_{1r} + ikp'_{1r} - k^2p_{1z}). \end{aligned} \quad (3.3)$$



(a) Free surface liquid jet

Figure 1: Definition of the coordinate system and the jet geometry. The jet is placed in a cylindrical coordinate system (r, θ, z) and its axis of symmetry is along the z -axis. The jet surface is defined by $r = \phi(z, t)$ and \mathbf{n} is the outward unit normal. Arrows indicate the polarity vector orientation.

The leading order linearized boundary conditions at $r = 0, 1$ are given by

$$v_{1r}(0) = 0, \quad v_{1r}(1) = \alpha\phi_1.$$

$$2v'_{1r}(0) + ikv_{1z}(0) = 0, \quad v'_{1r}(1) + v_{1r}(1) + ikv_{1z}(1) = 0,$$

$$p_{1r}(0) = 0, \quad p'_{1r}(1) = -\frac{1}{8}(p_{1r}(1) - ik\phi_1), \quad p'_{1z}(0) = 0, \quad p'_{1z}(1) = 0.$$

(3.4)

$$-\Pi_1(1) + 2\eta v'_{1r}(1) + 2\beta p'_{1r}(1) + \tau(k^2 - 1)\phi_1 = 0,$$

$$\left\{ (\eta + \frac{\gamma}{4}v(v-1))(ikv_{1r} + v'_{1z}) + \beta(ikp_{1r} + p'_{1z}) + (\zeta - \frac{i}{2}k(v-1)\gamma w + \frac{1}{2}(v-1)\gamma\lambda)p_{1r} \right.$$

$$\left. - \frac{\alpha}{2}\gamma(v-1)p_{1r} - \frac{v-1}{4}\gamma(v'_{1z} - ikv_{1r}) \right\} |_{r=1} - ik\zeta\phi_1 = 0.$$

Eqs. (3.2, 3.3, 3.4) constitute a linear boundary value problem of ordinary differential equation system. We solve this boundary value problem to obtain the dispersion relation $\alpha(k)$ and then to analyze the positive growth rates as functions of key model parameters and discuss their physical implications. Since an analytic solution is intractable for the system, we solve the boundary value problem consisted of linear ordinary differential equations together with the boundary conditions using a finite difference method numerically. The derivatives at the boundaries are discretized using one-sided differencing.

The parameters and their values used in this study are listed in Table 1. The resultant dimensionless parameters are given by:

$$\eta = 2, \tau = 10, \zeta = 1, \lambda = 0, w = 0, \beta = 1, \gamma = 1, v = 0.5, K = 1 \times 10^{-2}, h_1 = h_2 = 10. \quad (3.5)$$

In order to benchmark the results of the ALC jet, we study linear stability of a limiting passive liquid crystal jet firstly.

Table 1: Model Parameters

Symbol	Parameter	Value	Unit
t_0	Characteristic time scale	0.1	s
l_0	Characteristic length scale	1×10^{-3}	m
ρ_0	Density of the active liquid crystal solution	1×10^3	$kg \cdot m^{-3}$
η	Solvent viscosity	2×10^{-2}	$kg \cdot m^{-1} \cdot s^{-1}$
τ	Coefficient of surface tension	1×10^{-3}	$kg \cdot s^{-2}$
λ	Coefficient of self-propelled motion	0	s^{-1}
ζ	Coefficient of the bulk active stress	1×10^{-1}	$kg \cdot m^{-1} \cdot s^{-2}$
w	Speed of self-propelled motion of active particles	0	$m \cdot s^{-1}$
β	Generalized viscosity of ALC	1×10^{-4}	$kg \cdot s^{-2}$
γ	Rotational viscosity (relaxation parameter)	1×10^{-2}	$kg \cdot m^{-1} \cdot s^{-1}$
v	Geometric parameter of the active particle	$(-\infty, +\infty)$	1
K	Frank elastic constant	1×10^{-9}	$kg \cdot m \cdot s^{-2}$
h_1	Quadratic coefficient in the bulk free energy	1	$kg \cdot m^{-1} \cdot s^{-2}$
h_2	Quartic coefficient in the bulk free energy	1	$kg \cdot m^{-1} \cdot s^{-2}$
δ	Strength of boundary anchoring	$[0, +\infty)$	m^{-1}

3.1 Rayleigh instability of passive liquid crystal jets

When we set the active parameters zero: $\lambda = 0, \zeta = 0, w = 0, \beta = 0$, our model reduces to a model for passive liquid crystal jet without enforcing \mathbf{p} as a unit vector, which is valid at the defect. We note that Rey et al. studied the capillary instability of a passive liquid crystal jet using a lubrication theory based on the Ericksen-Leslie model and Rapini-Papoular equation and Fel and Zimmels studied it using the full Ericksen-Leslie model together with a long range surface elastic effect involving the Gaussian curvature [47, 48, 50]. Wang studied it using an orientation tensor based model [45, 46]. *Our study here is limited to a simplified kinetic boundary condition and a more general anchoring boundary condition to set the stage for benchmarking the results on ALC jets.* In addition to the numerical method for the full boundary value problem, we also employ an asymptotic method to derive an analytic expression for the positive growth rate and the cutoff wave number associated with the jet instability.

A classical simplifying assumption exploited here in the asymptotic approach is that the wavelength of the surface wave is much longer than that of the jet radius (a slender jet approximation or lubrication method) [47, 41, 42, 45]. So, in the long-wavelength approximation, the characteristic length scale in the r-direction is much smaller than that in the z-direction. At the leading order, the velocity perturbation is approximately given by $\delta \mathbf{v}(r, z, t) = (r \delta v_r(z, t), 0, \delta v_z(z, t))$, the free surface by $\phi = 1 + \delta \phi$ and the polarity vector by $\mathbf{p} = (0, 0, 1 + \delta p_z)$. A straight forward derivation yields an asymptotic model for the linearized system at $\delta = 0$, which is given in the Appendix. After applying the normal mode, the dispersion relation of the asymptotic model equation gives the following growth rate formula:

$$\alpha^* = \frac{\tau k^2 (1 - k^2)}{(3\eta + \gamma v^2) k^2 + \sqrt{(3\eta + \gamma v^2)^2 k^4 + 2\tau k^2 (1 - k^2)}}. \quad (3.6)$$

The liquid crystal jet is unstable when $0 < k < 1$ with a cutoff wave number at $k = 1$. This is known as the capillary or Rayleigh instability for liquid jets. The maximum growth rate α_{max}^* and

the corresponding wave number k_{max} is given, respectively, by:

$$\alpha_{max}^* = \sqrt{\tau} \left(2\sqrt{2} + 6A \right)^{-1}, \quad k_{max} = \left(\sqrt{2 + 3\sqrt{2}A} \right)^{-1}, \quad (3.7)$$

where $A = \frac{\eta + \frac{1}{3}\gamma^2}{\sqrt{\tau}}$ is the Ohnesorge number. In this approximate dispersion relation, the distortional elasticity K does not show up at all in the growth rate formula, indicating its role to the Rayleigh instability is negligible in this model. To confirm it, we conduct a numerical computation on the full linearized model and show that this approximate dispersion relation is extremely accurate in the range of unstable wave numbers $0 \leq k \leq 1$. Figure 2 shows the comparison between the approximate growth rate and the growth rate calculated from the full numerical computation. They are indeed indistinguishable in $k \in [0, 1]$. Outside the unstable wave number interval, however, we see visible deviation between the asymptotic result and the numerical one.

The asymptotic growth rate shows explicitly how the growth rate depends on the model parameters and the wave number. For the passive liquid crystal jet, the Frank elastic constant K has no effect to the positive growth rate (see Figure 2 (c).) Through extensive numerical experiments, we conclude that the boundary anchoring condition of \mathbf{p} at $r = 1$ also has no effect to the positive growth rate (see Figure 2 (d).) The positive growth rate only depends on viscosity η , relaxation parameter γ , geometric parameter v and the surface tension coefficient τ . The classical cutoff at $k = 1$ retains and the term $\frac{1}{3}\gamma^2$ acts as an additional material's viscosity. The maximum growth rate and the corresponding wave number only depends on the ratio between the effective viscosity and the surface tension. A higher viscosity reduces the growth rate while a higher surface tension promotes it. Since the molecular anisotropy is proportional to $|v|$, the more anisotropic of the liquid crystal molecule is, the smaller the growth rate is. So, the molecular anisotropy can in fact reduce the growth rate in the capillary instability. It follows from the Ericksen-Leslie theory that the Liquid crystal jet of tumbling liquid crystals (i.e., $|v| < 1$) is more unstable than that of flow-aligning liquid crystals ($|v| > 1$).

3.2 Linear instability of active liquid crystal jets

Next, we study the active liquid crystal jet to investigate how the activity parameterized by active parameters w , ζ and β can impact on the jet stability. We focus on the impact of the two activity parameters ζ and β primarily and remark on the role of w in the end. The upshot here is that both activity parameters ζ and β can have important and sometimes unexpected effect on stability of the active liquid crystal jet. Specifically, the active liquid crystal jet can be subject to three types of instabilities depending on values of the active parameters and the molecular geometric parameter v : (i). for a moderate value of ζ and any values of the other model parameters, the classical Rayleigh instability persists; however, the active parameter ζ can shift the cutoff wave number in the classical Rayleigh instability to induce additional unstable wave modes or to reduce or even suppress existing unstable wave modes, depending on the type of the molecular activity; (ii). the polarity vector instability inherent in the active matter system can be accessed in multiple modes in certain parameter regimes by the ALC jet or completely suppressed in other parameter regimes; (iii). the active viscous stress, when strong enough, can induce new instabilities in waves of intermediate wave numbers in certain parameter regimes. In the following, we will elaborate on the new instabilities and try to identify the parameter space where none, some or all of these instabilities exist.

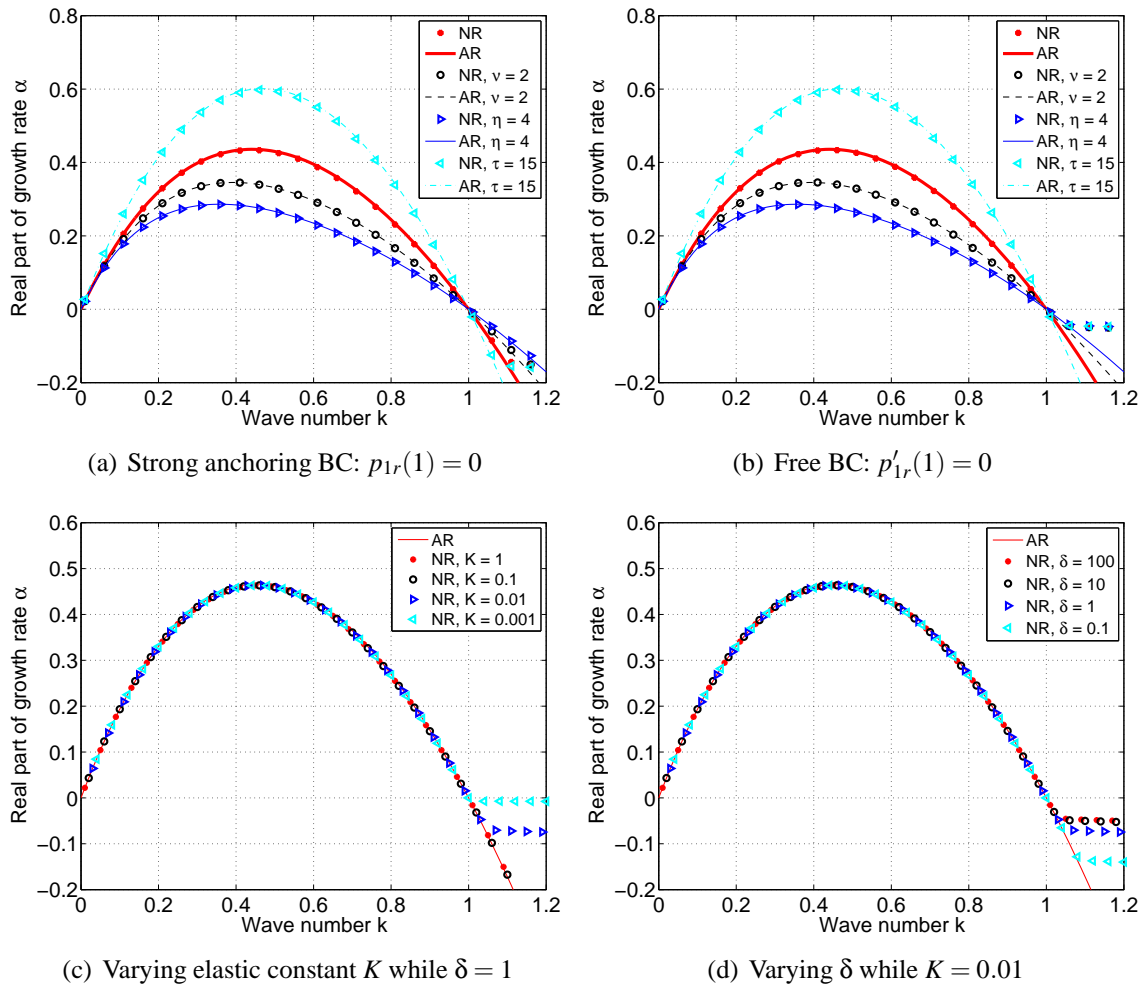


Figure 2: The growth rate of a passive liquid crystal jet as a function of the wave number at selected model parameters. NR represents the numerical result while AR does the analytic one. The values of the model parameters $K = 0.01$, $\eta = 2$, $\tau = 10$, $\nu = 1$, $\gamma = 1$, $\lambda = \zeta = w = \beta = 0$. The numerical results (dots) agree very well with the analytical ones (curves) in the range of unstable wave numbers. They may deviate away from each other in the stable wave number regime though.

(a). Growth rates at selected values of η, ν, τ with a strong anchoring condition at the interface.

(b). Growth rates at selected values of η, ν, τ with a free boundary condition at the interface.

(c). Growth rates at selected values of $K = 0.001, 0.01, 0.1, 1$ while $\delta = 1$.

(d). Growth rates at selected values of $\delta = 0.1, 1, 10, 100$ while $K = 0.01$. The growth rate is insensitive to K and δ in the unstable wave number regime. But, the growth rate becomes sensitive to the two model parameters in the stable wave number regime. So, Rayleigh instability in this model is primarily due to the jet surface tension, molecular geometry, its hydrodynamic properties and short-range elastic properties other than its long-range elastic properties and the boundary anchoring condition.

We note that active stress $\zeta \mathbf{pp}$ describes the force exerted by active particles on the surrounding fluid. That the local flow generated by the active particles is extensile or contractile is determined by the sign of ζ [58]. It is extensile if $\zeta < 0$; in this case the active particles/molecules are called pushers. It is contractile if $\zeta > 0$; in this case the active particles/molecules are called pullers.

3.2.1 Bulk activity induced polarity vector instability

Firstly, we consider the effect of the bulk active stress term $\zeta \mathbf{pp}$ to the ALC jet by setting $w = 0, \beta = 0$. In this study, we want to evaluate the role of the inherent polarity vector instability, previously identified in the ALC material in unconfined domains in long to intermediate wave lengths, when coupled with flows in the jet. We remark that this inherent instability belongs to the unstable mode accessed by a perturbation transverse to the primary polarity direction and is therefore different from the unstable mode studied in [32]. We begin with the investigation in the zero wave number limit ($k = 0$) with a strong anchoring boundary condition ($\delta = 0$), where the governing equations for the linearized boundary value problem can be simplified significantly.

The component p_{1z} in the linearized system is decoupled from the rest of the equations and solely governed by a Bessel equation

$$r^2 p''_{1z} + r p'_{1z} - B r^2 p_{1z} = 0, \quad (3.8)$$

where $B = \frac{\alpha\gamma + 2h_2}{K}$. Note that only if $B < 0$ (i.e., $\alpha < -\frac{2h_2}{\gamma}$), the Bessel equation can have a nontrivial, real solution corresponding to $p'_{1z}(0) = 0, p_{1z}(1) = 0$. So, there does not exist any instability associated with the perturbation on p_z .

If there is any instability, it must be given by the coupled equations for p_{1r} and v_{1z} . The governing equations for these components are given by

$$\alpha p_{1r} = \frac{K}{\gamma} (p''_{1r} + \frac{1}{r} p'_{1r} - \frac{1}{r^2} p_{1r}) + \frac{\nu-1}{2} v'_{1z}, \quad (3.9)$$

$$\alpha v_{1z} = \eta (v''_{1z} + \frac{1}{r} v'_{1z}) + \zeta (\frac{p_{1r}}{r} + p'_{1r}) - \frac{\alpha}{2} \gamma (\nu - 1) (\frac{p_{1r}}{r} + p'_{1r}) + \frac{1}{4} \gamma (\nu - 1)^2 (\frac{v'_{1z}}{r} + v''_{1z}).$$

If we assume additionally that K is small, it follows from eq. (3.9) that

$$r^2 p''_{1r} + r p'_{1r} + (A r^2 - 1) p_{1r} = 0 \quad (3.10)$$

together with the boundary conditions

$$p_{1r}(0) = 0, \quad p_{1r}(1) = 0, \quad (3.11)$$

where $A = \frac{-2\alpha^2}{2\alpha\eta + \zeta(\nu-1)}$. In this case, the Bessel equation has nonzero real solutions only if $A > 0$. Then, from the definition of A ,

$$\frac{2}{A} \alpha^2 + 2\eta\alpha + \zeta(\nu-1) = 0. \quad (3.12)$$

If $\zeta(\nu-1) < 0$, the equation has a root $\alpha = -\frac{\eta A}{2} + \frac{1}{2} \sqrt{\eta^2 A^2 - 2\zeta A(\nu-1)} > 0$. Otherwise, $\alpha \leq 0$. The solution of the Bessel equation satisfying $p_{1r}(0) = 0$ is given by

$$p_{1r} = C_1 J_1(\sqrt{A}r), \quad (3.13)$$

where C_1 is an arbitrary constant and J_1 is the Bessel function of the first kind. Using $p_{1r}(1) = 0$, we have $\sqrt{A} = \xi_n, n = 1, 2, \dots$, where ξ_n are the positive roots of Bessel function $J_1(\xi)$. Then, the growth rates can be represented by the roots as follows:

$$\alpha_n = -\frac{1}{2}\eta\xi_n^2 + \frac{1}{2}\sqrt{\eta^2\xi_n^4 - 2\zeta(\nu-1)\xi_n^2}, n = 1, 2, \dots \quad (3.14)$$

Since $\xi_n \rightarrow +\infty$, $\alpha_n \rightarrow -\frac{\zeta(\nu-1)}{2\eta}$ as $n \rightarrow \infty$. This shows that there exists infinitely many positive growth rates α_n in the limit of $K \rightarrow 0^+$.

For other boundary conditions parameterized by $\delta > 0$, even though we can't obtain an analytical result asymptotically, we still find strong evidence to support the existence of infinitely many $\alpha_n \sim -\frac{\zeta(\nu-1)}{2\eta}$, as $n \rightarrow \infty$ if the wave number k is small and the elastic constant K is small numerically. We list our numerical results in Table 2 for all three types of boundary conditions with $-\frac{\zeta(\nu-1)}{2\eta} = 1.5$ at a few selected values of δ . From the numerical results, we conclude that $\alpha_n \rightarrow -\frac{\zeta(\nu-1)}{2\eta}$ as $K \rightarrow 0^+$ and $n \rightarrow \infty$.

The model parameters used for producing Table 2 are $\zeta = 4, \nu = -0.5, \eta = 2, \tau = 10, \gamma = 1, \lambda = w = \beta = 0$. Table 2 also lists the growth rates at a few selected values of δ to see how the anchoring boundary condition at the free surface affects the instability. If δ is small, the result of the soft anchoring BC is very close to that of the strong anchoring BC; if δ is large, the result of the soft anchoring BC is close to that of the Neumann (free) BC.

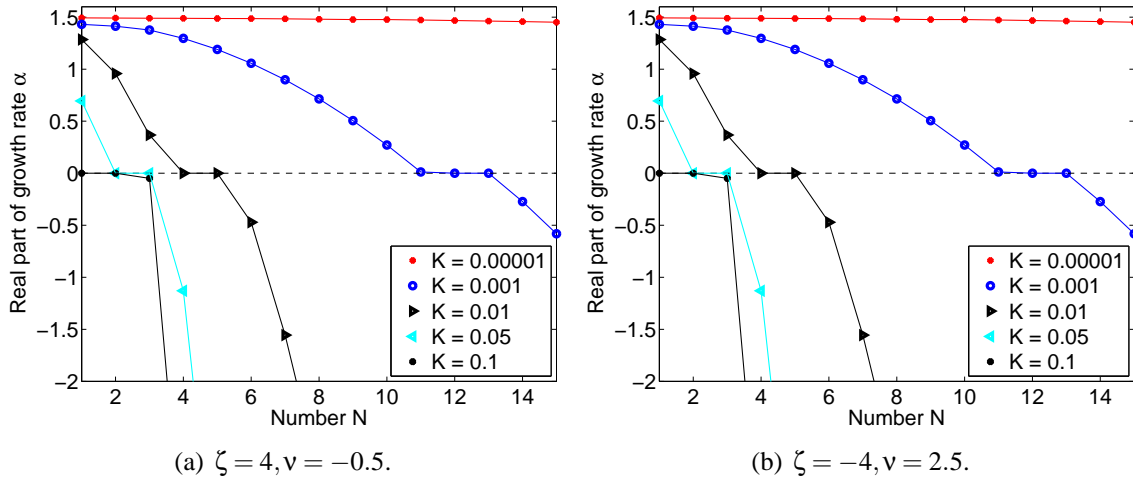


Figure 3: The effect of the Frank elastic constant K at a small wave number $k = 0.00001$. The model parameters are $\eta = 2, \tau = 10, \gamma = 1, \delta = 0.1, \lambda = w = \beta = 0$. N is the number of first N largest growth rates at the wave number calculated numerically. When the growth rates fall below the lower bound in the figure, they are not shown. As the long-range distortional elasticity enhances, the instability can be suppressed completely. This mode of instability is termed the polarity vector instability owing to the coupling between the polarity field and the flow field. (a). Growth rates of active discotic liquid crystal jets. (b). Growth rates of active rodlike liquid crystal jets. The quantity $-\frac{\zeta(\nu-1)}{2\eta} = 1.5$ is identical in both (a) and (b). So are the corresponding growth rate curves in (a) and (b).

When the Frank elastic constant is not negligibly small, our numerical studies show that the role of the distortional elasticity is to reduce the growth of the unstable modes and therefore has

the tendency to stabilize the jet. Figure 3 plots the first 15 largest real parts of the eigenvalues (ordered by the magnitude) of the full linear system at a very small wave number ($k = 0.00001$). The maximum real part of the eigenvalues decreases when the Frank elastic constant (K) increases. If K is small enough, the maximum is well approximated by 1.5 (for the model parameters given above). If K is larger than some critical value K_c , the real parts of the eigenvalues are negative, demonstrating the stabilizing effect of the distortional elasticity. If K (small) and $\nu < 1$ are fixed, there exists a critical value of $\zeta_c > 0$ such that there are eigenvalues with positive real parts only if $\zeta > \zeta_c$. Similarly, if $\nu > 1$ is fixed, there exists a critical value $\zeta_c < 0$ such that there are eigenvalues with positive real parts only when $\zeta < \zeta_c$. We note that the results are identical for the two group parameters $\zeta = 4, \nu = -0.5$ and $\zeta = -4, \nu = 2.5$ which yield the same value: $\zeta(\nu - 1) = -6$. This clearly suggests that there exist a relationship between the geometry of the active liquid crystal particle and the strength of the activity in this instability. We then, numerically calculate the stable vs unstable regions in the parameter space (ζ, ν) and plot it in Figure 4 for various boundary conditions parameterized by δ and the Frank elastic constant K .

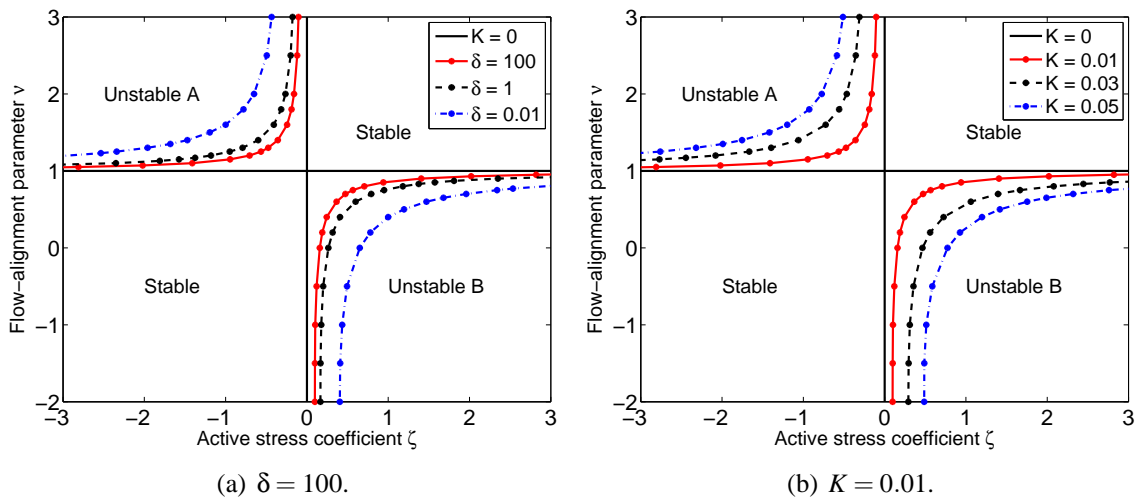


Figure 4: The stable vs unstable region in parameter space (ζ, ν) in the zero-wave number limit for the polarity vector instability. The values of the model parameters are $\eta = 2, \tau = 10, \gamma = 1, \lambda = w = \beta = 0$. (a). The curves depict the critical values ζ_c as a function of ν , which define boundaries between the stable and the unstable region with respect to selected values of $K = 0, 0.01, 0.03, 0.05$ at $\delta = 100$. Clearly, enhanced distortional elasticity can reduce the size of the unstable region and thereby stabilize the jet due to this instability. (b). The curves depict the critical values ζ_c as a function of ν , which define boundaries between the stable and the unstable region with respect to selected values of $\delta = 0.1, 1, 10, 100$ at $K = 0.01$. The strengthening anchoring boundary condition can also reduce the size of the unstable region in the parameter space. The results indicate that the long-wave instability is possible only for pushers with a geometric feature that promotes flow-aligning ($\nu > 1$) and pullers with a geometric feature that promotes tumbling or of a discotic shape ($\nu < 1$).

From this study, we conclude that if $\zeta(\nu - 1) > 0$, the instability is completely suppressed; if $\zeta(\nu - 1) < 0$, there can exit critical values ζ_c and K_c such that the instability can incur if $|\zeta| > |\zeta_c|$ and $K < K_c$, where the maximum growth rate is achieved at the zero wave number $k = 0$

with its value bounded by $-\frac{\zeta(\nu-1)}{2\eta}$. For all model parameters that we have explored, we record monotonically decreasing growth rate curves as functions of the wave number k . Figure 5 depicts a set of growth rate curves at selected model parameters, where the monotonically decreasing curves represent the growth rates corresponding to the instability. Looking forward, when $\beta \neq 0$, the monotonicity of the growth rate curve may be lost. We will discuss the case in the last subsection when we consider the combined effect of ζ and β .

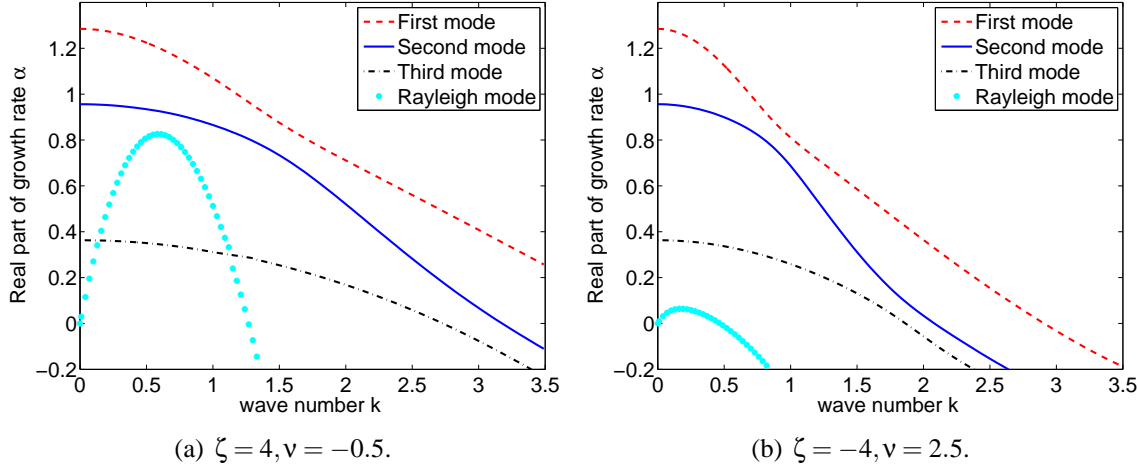


Figure 5: Growth rate curves of three unstable polarity vector modes together with the Rayleigh mode. The growth rates for the polarity vector instability are decreasing functions of the wave number k . The parameter values are $K = 0.01, \eta = 2, \tau = 10, \gamma = 1, \delta = 0.1, \beta = 0, \lambda = w = \beta = 0$. (a). Growth rates of active discotic liquid crystal jets. (b). Growth rates of active rodlike liquid crystal jets.

This instability is tied to polarity vector and hydrodynamic interaction via the bulk active stress parameterized by ζ , which is obviously absent in passive liquid crystal limit. From the asymptotic formula for growth rate, we can trace it back to the inherent instability in the active liquid crystal in an infinite domain, where a single unstable mode exists in the direction transverse to the orientation of the underlying steady state polarity vector. In the context of an axisymmetric, cylindrical jet, however, the single unstable mode can be amplified to encompass infinitely many unstable modes in some cases when Franks elasticity is weak ($K \ll 1$) or completely suppressed in others for larger K . This instability is unique to the active liquid crystal jet.

3.3 Activity modified Rayleigh instability

For the active liquid crystal jet flow, the classical Rayleigh instability persists in a finite wave number interval $0 < k < k_{cutoff}$ at a moderate value of ζ , where k_{cutoff} is the cutoff wave number equal to 1 for isotropic fluid and passive liquid crystal flows, but depends on model parameters for active liquid crystal flows. *When focused exclusively on the Rayleigh mode, the result is striking: the bulk active stress (parametrized by ζ) can shift the cutoff wave number. If $\zeta > 0$, the cutoff wave number is shifted to the right ($k_{cutoff} > 1$) so that more waves becomes unstable; whereas if $\zeta < 0$, the cutoff wave number is shifted to the left ($k_{cutoff} < 1$) so that less waves are unstable. E.g.,*

for an active liquid crystal system consisting of pullers and pushers, pullers tend to destabilize the jet while pushers tend to stabilize it. This result is shown in the growth rate curves depicted in Figure 6 for both the discotic and rodlike active liquid crystals. We point out that the anchoring boundary condition of \mathbf{p} at $r = 1$ and the Frank elastic constant K have little or no effect to this unstable mode analogous to the case of the passive liquid crystal jet flow. The growth rate depends on v in this unstable mode via $|v|$, demonstrating a symmetry with respect to the geometry of the molecule. Moreover, the growth rate decreases as the geometric parameter increases in its magnitude, confirming the anisotropy in the molecular geometry has the impact of reducing the growth. Figure 7 depicts the sensitivity of the growth rate as a function of the geometric parameter v and its symmetry with respect to the geometry of molecules.

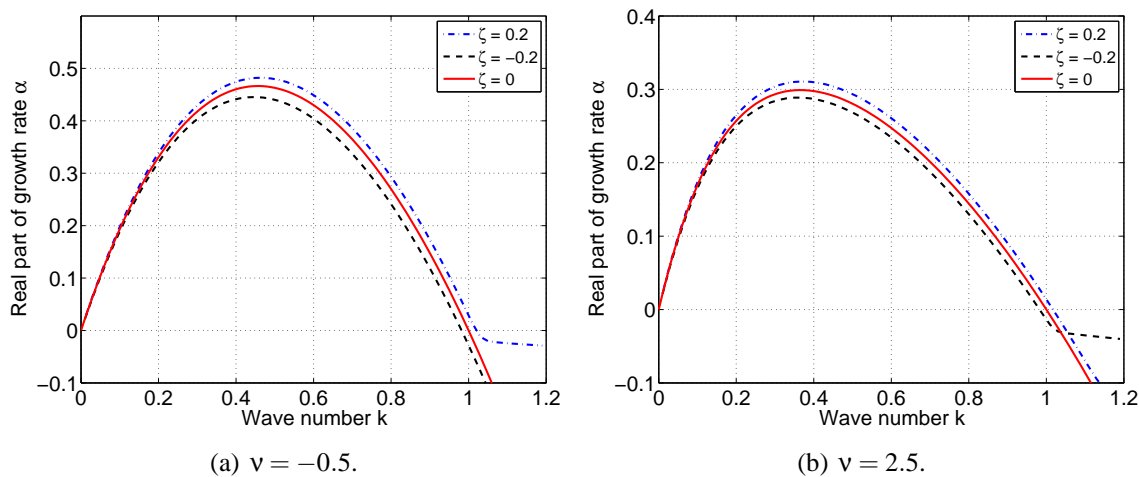


Figure 6: Growth rates in the unstable Rayleigh mode. The model parameter values are $K = 0.01, \eta = 2, \tau = 10, \gamma = 1, \lambda = w = \beta = 0, \delta = 1$. A positive ζ shifts the cutoff wave number to the right ($k_{cutoff} > 1$) while a negative ζ shifts it to the left ($k_{cutoff} < 1$). The cutoff wave number grows and decays monotonically with respect to ζ . While the cutoff wave number shifts, the wave number corresponding to the peak of the growth rate also shifts with respect to ζ . Hence, the pusher has the tendency to stabilize the jet while the puller destabilizes it. (a). The growth rate of an active discotic liquid crystal jet at $\zeta = -0.2, 0, 0.2$, respectively. (b). The growth rate of an active flow-aligning rodlike liquid crystal jet at $\zeta = -0.2, 0, 0.2$, respectively.

The activity parameter ζ together with the other model parameters in Figure 6 can be chosen to be in the stable region in Figure 4 to suppress the polarity vector instability so that the Rayleigh mode is the only unstable mode for the jet flow. We choose this case to highlight the new feature in the Rayleigh instability. We note that the cutoff wave number in the Rayleigh instability is independent of the flow-aligning parameter v although it depends on the activity parameter ζ (see Figure (7)).

When values of (ζ, v) are located in the unstable region in Figure 4, the polarity vector instability shows up besides the Rayleigh instability (see Figure 8). As alluded to earlier, the polarity vector instability depends strongly on the Frank elastic constant K and the BC of p_{1r} at $r = 1$ even when it coexists with the Rayleigh mode.

In the Rayleigh mode, for pushers ($\zeta < 0$), the cutoff wave number reduces as the magnitude $|\zeta|$ increases. If $\zeta < 0$ is sufficiently small (i.e., $|\zeta|$ is large enough in magnitude), it may suppress

Table 2: Growth rates calculated numerically

BC at $r = 1$	$p_{1r}(1) = 0$	$\delta = 0.01$	$\delta = 1$	$\delta = 100$	$p'_{1r}(1) = 0$
Max of $\text{Re}(\alpha)$ at $K = 0.00001$	1.4920	1.4921	1.4950	1.4960	1.4960
Max of $\text{Re}(\alpha)$ at $K = 0.01$	1.2522	1.2557	1.3755	1.4098	1.4102
Max of $\text{Re}(\alpha)$ at $K = 0.05$	0.5362	0.5540	1.0898	1.2395	1.2413
Max of $\text{Re}(\alpha)$ at $K = 0.2$	0	0	0.0175	0.6053	0.6124
Max of $\text{Re}(\alpha)$ at $K = 0.5$	0	0	0	0	0

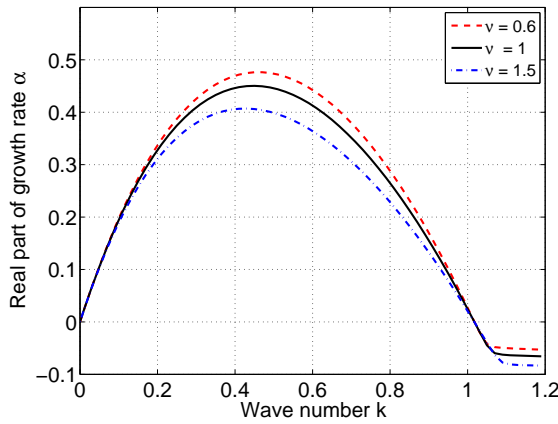
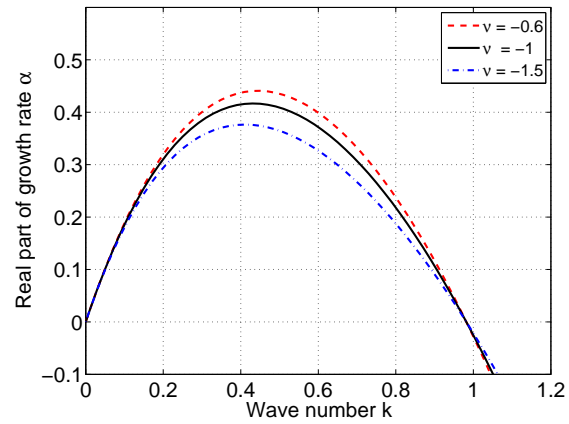
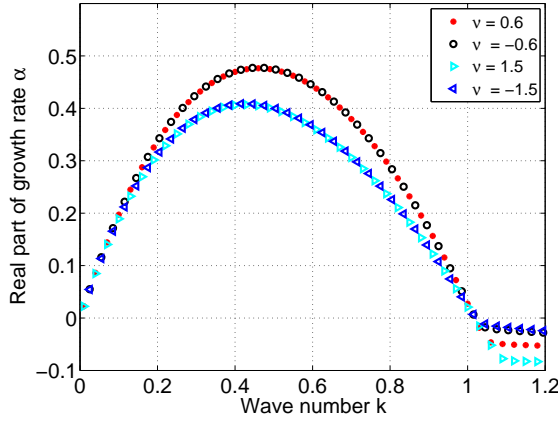
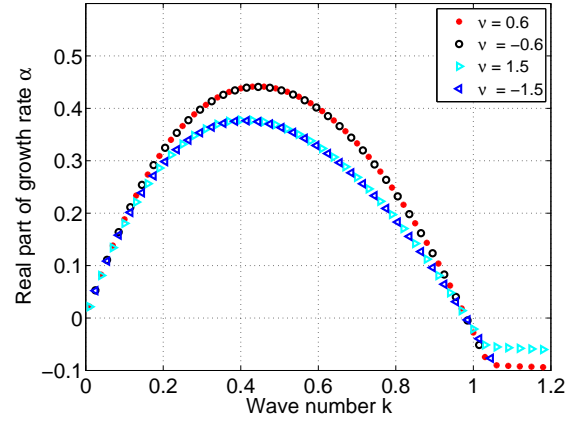
(a) $\zeta = 0.2$.(b) $\zeta = -0.2$.(c) $\zeta = 0.2$.(d) $\zeta = -0.2$.

Figure 7: Sensitivity of the unstable Rayleigh growth rate to v with the weak anchoring BC. The model parameter values are $K = 0.01$, $\eta = 2$, $\tau = 10$, $\gamma = 1$, $\lambda = w = \beta = 0$, $\delta = 1$. The enhancement in geometric anisotropy can reduce the growth rate. (a). Pullers. (b). Pushers. The growth rate only depends on $|v|$ in the unstable region for both pullers (c) and pushers (d).

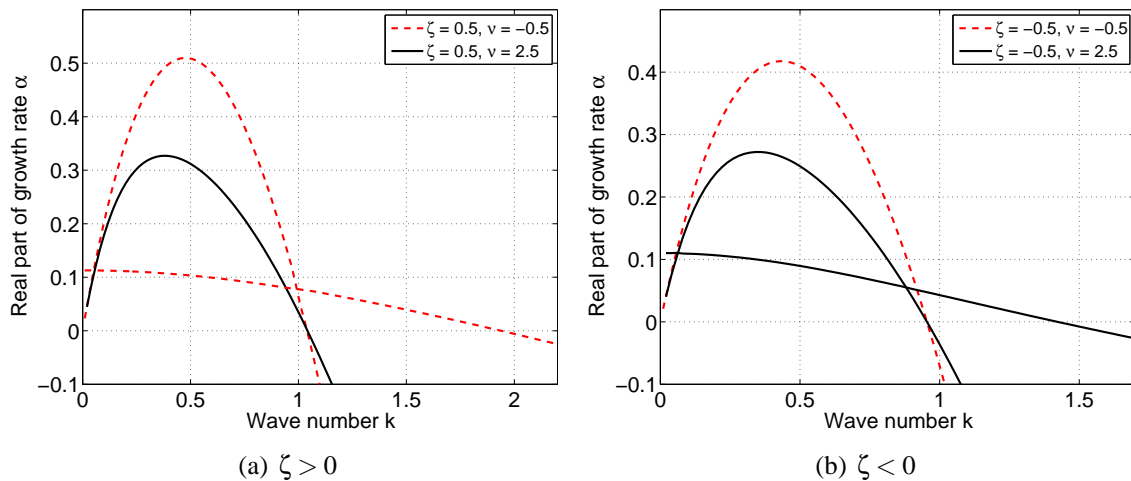


Figure 8: Sensitivity of the unstable Rayleigh growth rate together with the unstable polarity vector growth rate with respect to v . The model parameter values are $K = 0.01, \eta = 2, \tau = 10, \gamma = 1, \lambda = w = \beta = 0, \delta = 1$. The cutoff wave number is independent of v while the peak of the growth curve is not. The growth rates in the unstable Rayleigh mode depend completely on $|v|$, demonstrating a complete symmetry with respect to v . The growth rates in the unstable polarity vector mode in (a) and (b) overlap because $\zeta(v - 1)$ is identical in the rodlike liquid crystal and the discotic one shown.

the classical Rayleigh instability completely! Figure (9-a) depicts such a scenario where $v < 1$ and there does not exist any positive growth rates at $\zeta = -6$. Hence, if $v < 1$ and $\zeta < 0$ is small enough, all unstable modes can be completely suppressed leading to a stable jet! If $v > 1$ and $\zeta < 0$ is small enough, the Rayleigh's unstable mode can be suppressed, but the unstable polarity vector modes near the zero wave number limit survive; so, the jet is still unstable due to the polarity vector instability. Figure 9-b depicts the scenario where the Rayleigh instability is suppressed while the polarity vector instability persists.

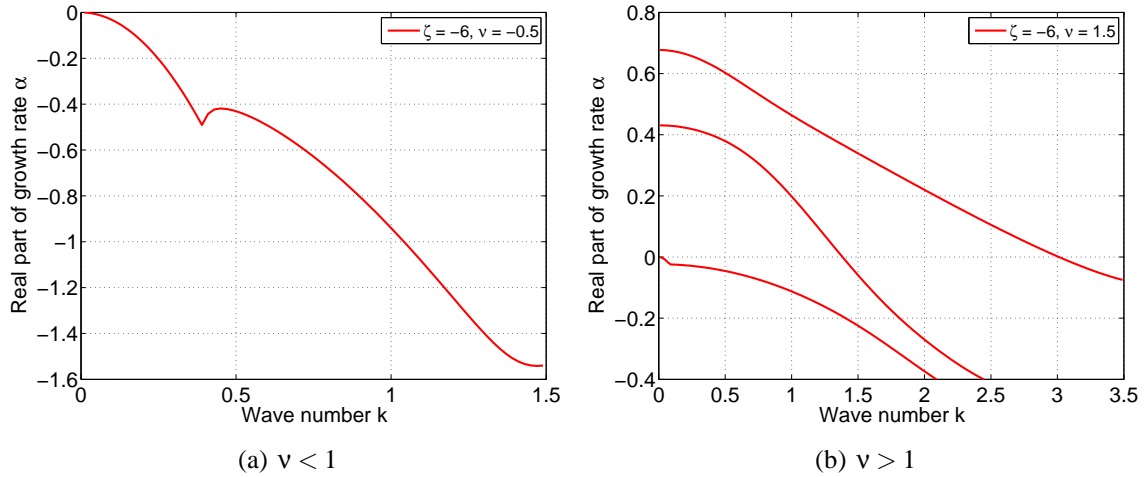


Figure 9: Suppression of the Rayleigh capillary instability due to a large activity. The model parameter values are $K = 0.01, \eta = 2, \tau = 10, \gamma = 1, \lambda = w = \beta = 0, \delta = 1$. (a). Rayleigh instability along with all other instabilities are completely suppressed leading to a stable jet. (b). Rayleigh instability is suppressed while unstable polarity vector modes persist for long-waves.

3.4 Active viscous stress induced instability

Finally, we examine how active viscous stress $\beta(\nabla\mathbf{p} + \nabla\mathbf{p}^T)$ impacts on stability of an active liquid crystal jet. Firstly, we set the self-moving velocity $w\mathbf{p}$ and the bulk active stress $\zeta\mathbf{pp}$ term to zero to suppress the polarity vector instability and highlight the role played by the active viscous stress. An interesting result shows up: in addition to the Rayleigh's unstable mode already discussed, another window of instability may emerge in the intermediate wave number regime whose wave number is larger than that of the Rayleigh's. This mode of instability only shows up when the strength of the active viscosity is strong enough regardless if it is positive or negative and $v < 1$. In fact, the growth rate depends on $|\beta|$ and there exists a β_c that depends on v such that if $|\beta| > \beta_c$, the new instability emerges together with the Rayleigh's unstable mode. As $|\beta| > \beta_c$ increases, the growth rate in this new unstable mode increases as well. Figure 10 (a) depicts the most unstable growth rate together with the unstable Rayleigh mode at a few selected values of β , in which the new instability emerges at $\beta = 3$ and is suppressed at smaller values of β . The active viscous stress seems to affect the growth rate in the unstable Rayleigh mode by increasing the growth rate in the mode as $|\beta|$ increases (shown in Figure 10(a).) When $v > 1$, i.e., the ALC jet is consisted of flow-aligning rods, the active viscous stress will not induce any instabilities and an increase in values of $|\beta|$ can in fact decrease the growth rate in the Rayleigh mode (see Figure 10(b).)

We next consider the combined effect of the bulk active stress $\zeta(\mathbf{pp})$ and the active viscous stress $\beta(\nabla\mathbf{p} + \nabla\mathbf{p}^T)$. Firstly, we examine the case for ALC jet consisting of pullers, i.e., $\zeta > 0$. If $v > 1$, the polarity vector instability is suppressed and the active viscous stress does not induce any new instability at all so that the Rayleigh mode may be the only existing unstable mode. Although the active viscous stress does not induce any new instabilities, it plays the role of reducing the cutoff wave number in the Rayleigh instability and thereby lowering the growth rate, an effect completely opposite to that of the bulk active stress with $\zeta > 0$. Figure 11(b) depicts the "stabilizing" effect of active viscosity β , where β shifts the cutoff wave number to smaller than 1 at $\beta = 2.4$. Once again,

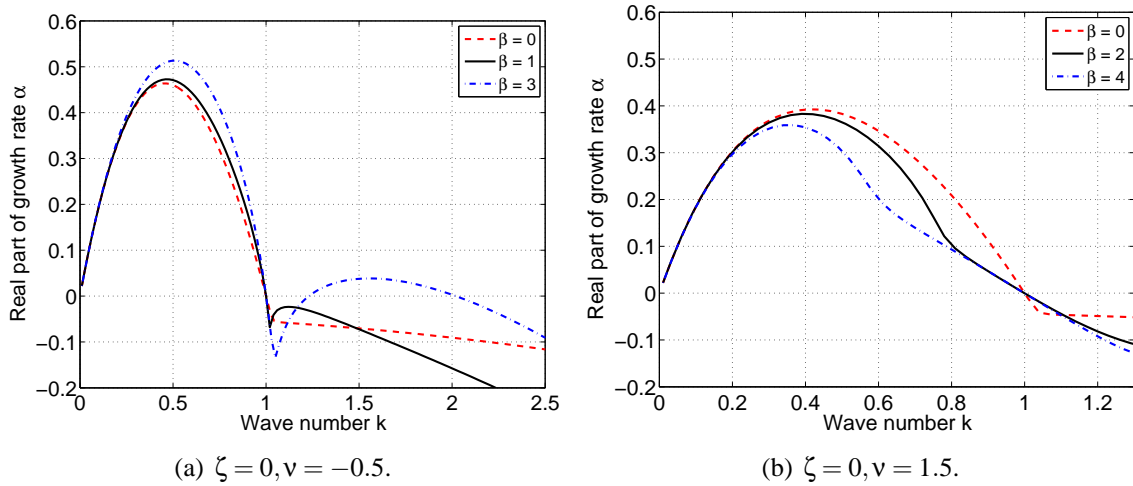


Figure 10: Growth rates of ALC jets at $\zeta = 0$ and a few selected values of β . The model parameter values are $K = 0.01, \eta = 2, \tau = 10, \nu = -0.5, \gamma = 1, \lambda = \omega = 0, \delta = 100$. (a). Growth rates of the unstable Rayleigh mode and the active viscous stress induced mode at $\nu < 1$. There exists a critical value β_c such that if $0 < |\beta| < \beta_c$, the unstable Rayleigh mode is the only unstable mode; for $|\beta| > \beta_c$, an additional instability may emerge in a wave number interval beyond that of the unstable Rayleigh mode's. The active viscous stress can not only induce an additional instability, but also increase the growth rate in the unstable Rayleigh mode. The growth rate depends only on $|\beta|$. (b). Growth rates of the unstable Rayleigh mode at $\nu > 1$. In this case, the Rayleigh mode is the only unstable mode. An increase in values of $|\beta|$ decreases the growth rate.

the growth rate depends on $|\beta|$ instead of β directly.

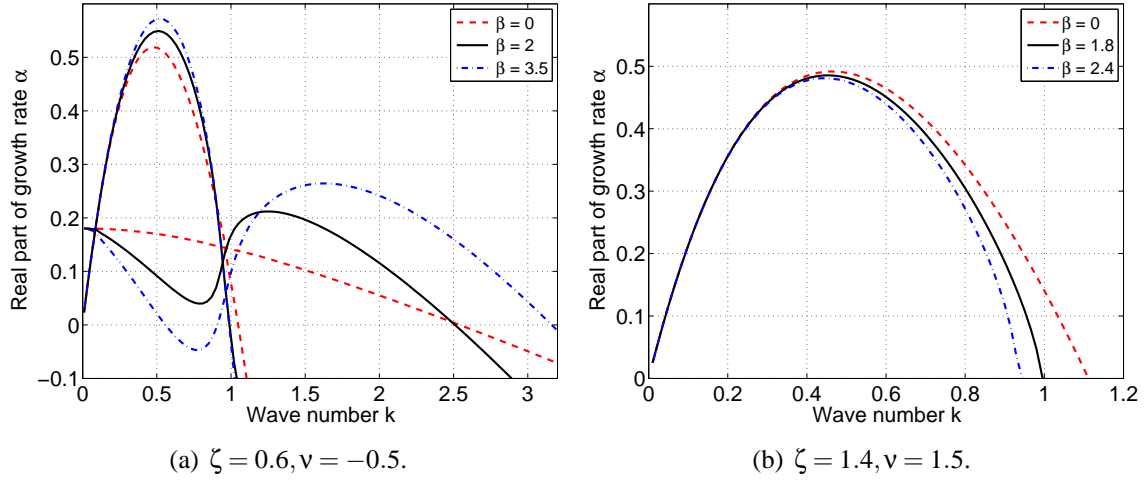


Figure 11: Unstable growth rates for ACL jets consisting of pullers. The model parameter values are $K = 0.01$, $\eta = 2$, $\tau = 10$, $\gamma = 1$, $\lambda = w = 0$, $\delta = 100$. (a). Case of $v < 1$. All three unstable modes may coexist. The role of $|\beta|$ is to reduce the growth rate for the polarity vector mode while promote the growth rate in the active viscous stress induced unstable mode. In the meantime, it increases slightly the Rayleigh growth rate. (b). Case of $v > 1$. The Rayleigh mode is the only unstable mode. The active viscous stress actually reduces the growth rate and shifts the cutoff wave number to smaller wave numbers, playing a role completely opposite to that of the bulk active stress ζ_{pp} .

If $v < 1$, $\zeta(v - 1) < 0$, where the polarity vector instability may exist in addition to the Rayleigh instability. The active viscous stress can reduce the unstable polarity vector mode in small wave number region and in the meantime induce a new instability in regions of intermediate wave numbers shown in Figure 11(a). In Figure 11(a), the growth rate due to the polarity vector instability actually breaks up into polarity vector unstable mode which decays with respect to $|\beta|$ and the new, active viscous stress induced unstable mode, which grows with respect to $|\beta|$. As we vary v , the growth rate curve due to the polarity vector instability may decay to partially negative so that the new mode emerges as a separate unstable window in the wave number space shown in Figure 10(a). At the presence of nonzero active viscosity, the monotonicity in the polarity vector growth rate curves is lost. In Figure 11(a), the growth rate curves for the polarity vector mode decrease only in the range of small wave numbers; they then turn around to become increasing, crossing the Rayleigh growth rate curve, and then become decreasing again in the range of intermediate wave numbers, creating a local maximum for the new mode that we call the active viscous stress induced unstable mode. If the two windows of instability for the two unstable modes are well separated in the case of large $|\beta|$, the distinction is apparent. Otherwise, it's difficult to define the boundary between the two unstable modes in the joined window of instability.

Secondly, we look at the ALC jet consisting of pusher molecules ($\zeta < 0$.) If $v > 1$, there exist two critical values of ζ , ζ_c and ζ_R . When $0 > \zeta > \zeta_c$, the Rayleigh's mode is the only unstable mode. For $\zeta_c > \zeta > \zeta_R$, there may coexist the unstable polarity vector and Rayleigh mode. For $\zeta_R > \zeta$, the unstable Rayleigh mode is suppressed so that only the unstable polarity vector mode survives. The details can be tabulated in the following.

1. If $0 > \zeta > \zeta_c$, the active viscous stress does not induce any new instabilities. Rayleigh mode is the only unstable mode. $|\beta|$ changes growth rate curve of the Rayleigh mode by increasing the cutoff wave number and meanwhile reducing the growth rate, see Figure 12(a).
2. If $\zeta_c > \zeta > \zeta_R$, there is no new instability due to the active viscosity β . An increase in values of $|\beta|$ reduces the growth in the unstable polarity vector mode while increasing the cutoff wave number for the Rayleigh mode. Figure 12(b) depicts the growth rates corresponding to the two unstable modes.
3. If $\zeta_R > \zeta$, the Rayleigh instability is suppressed and the polarity vector instability is the only survival unstable mode. An increase in values of $|\beta|$ apparently reduces the growth rate (see Figure 12(c)).

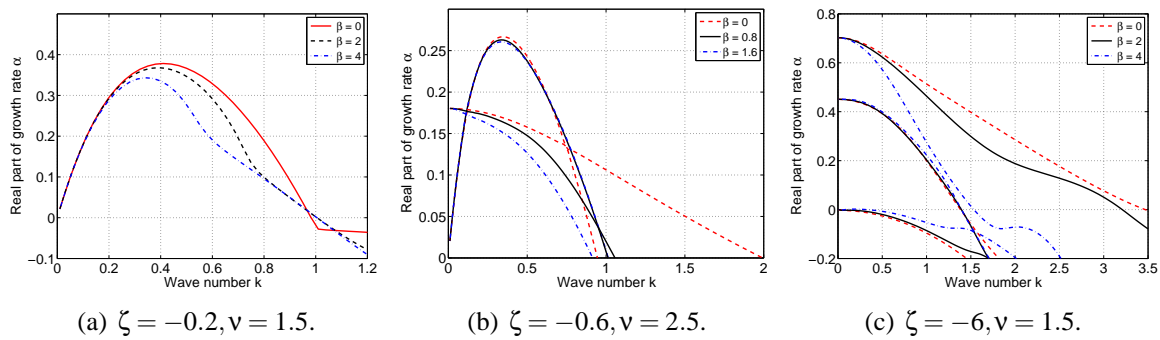


Figure 12: Growth rates at selected values of β for $\zeta < 0$ and $v > 1$. The model parameter values are $K = 0.01, \eta = 2, \tau = 10, \gamma = 1, \lambda = w = 0, \delta = 100$. (a). In this parameter regime, only Rayleigh instability exists. (b). In this parameter regime, the Rayleigh and the polarity vector instability coexist. (c). In this regime, only the polarity vector instability exists.

If $v < 1$, the polarity vector instability is completely suppressed. There exists a critical value ζ_R such that if $0 > \zeta > \zeta_R$, the unstable Rayleigh mode together with an active viscous stress induced unstable mode can coexist. For $\zeta_R > \zeta$, the Rayleigh's unstable mode is suppressed so that the active viscous stress induced mode may be the sole unstable mode. Specifically, we summarize the details below.

1. For $0 > \zeta > \zeta_R$, there exists a β_c such that the active viscous stress induced instability emerges when $|\beta| > |\beta_c|$ in addition to the unstable Rayleigh mode. Figure 13(a) depicts the growth rates corresponding to the two unstable modes.
2. For $0 > \zeta > \zeta_R$ and $|\beta| < \beta_c$, the Rayleigh mode is the only unstable mode. An increase in values of $|\beta|$ shifts the cutoff wave number to the right, making more waves unstable, and in the meantime slightly elevate the growth rate in the unstable Rayleigh mode. Figure 13(b) depicts the Rayleigh growth rate curve at three selected values of β .
3. For $\zeta_R > \zeta$, there exists a β_c such that the active viscous stress induced instability gives the only unstable mode when $|\beta| > |\beta_c|$. Figure 13(c) shows the growth rate variation with respect to three selected values of β .

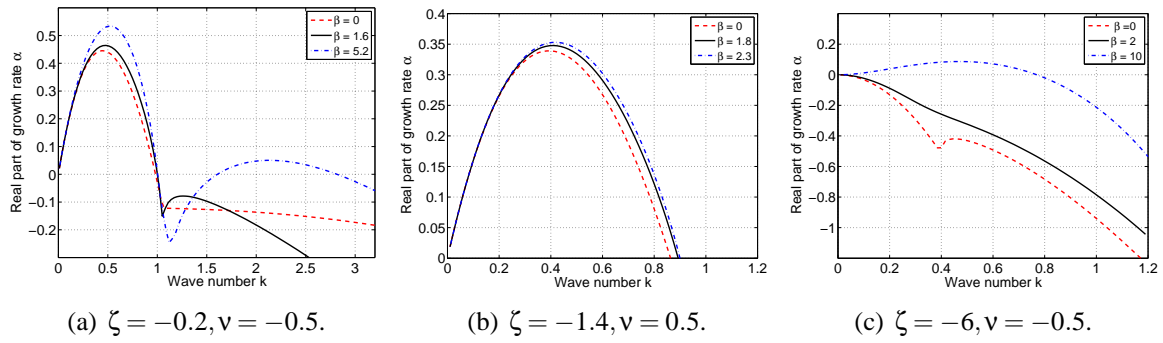


Figure 13: Growth rates at selected values of β for $\nu < 1$ and $\zeta < 0$. The values of parameters are $K = 0.01, \eta = 2, \tau = 10, \gamma = 1, \lambda = w = 0, \delta = 100$. (a). Case of $0 > \zeta > \zeta_R$ and $|\beta| > \beta_c$. Two unstable modes may coexist. (b). When the Rayleigh mode is the only unstable mode at $0 < |\beta| < \beta_c$, the active viscous stress shifts the cutoff wave number to the right to make more waves unstable, meanwhile elevates the growth rate in the unstable Rayleigh mode. (c). Case of $\zeta_R > \zeta$. Only the active viscous stress induced instability exists at a sufficiently large $|\beta|$.

Finally, we comment on the role of the self-propelling velocity parameterized by w . We have conducted extensive numerical studies and found that it changes the growth rate of the unstable modes marginally. When either of w or β are nonzero in the model, the imaginary part of the growth rates can be nonzero indicating the existence of propagating waves associated with some of the unstable modes.

In summary, the active viscous stress can induce new instability only when $\nu < 1$. In the case of $\nu > 1$, the role of active viscosity to the growth rate seems to be opposite to that of ζ in that while nonzero ζ shifts the cutoff wave number in the Rayleigh mode, β shifts it to the opposite direction. An increase in $|\beta|$ in general reduces the growth rate in the Rayleigh and the polarity vector mode. In the case of $\nu < 1$, it reduces the growth rate in the polarity vector mode for long waves while elevating the growth rate in the Rayleigh mode, and in the meantime, induces a new instability for intermediate waves. A quantitative study on how these active parameters impact on the jet stability in a detailed phase diagram for (ν, ζ, β) will be time consuming and postponed to a future study. Figure 12-c seems to suggest that the polarity vector instability and the active stress induced instability are in fact given by the same growth rate curve; therefore, they belong to the same unstable mode. However, when the Rayleigh instability is present, it is clearly shown in our numerical analysis that they belong to two separate families of growth rates. Thereby, it is indiscernible from our numerical analysis carried out here that if they are the same mode. Physically, they are clearly related to two separate mechanisms. In light of this, we will describe the instability induced by the active viscous stress as a new mode of instability, maybe more accurately, a new mechanism of instability.

4 Conclusion

We have studied linear stability of an infinitely long axisymmetric, cylindrical active as well as passive liquid crystal jet with a focus on the torsionless disturbances. Three unstable modes associated with the activities are identified: the polarity vector mode, the modified Rayleigh mode,

and the active viscous stress induced unstable mode. First of all, the bulk active parameter ζ and the active viscosity β can both affect the Rayleigh instability in such a way that the cutoff wave number and the growth rate can be modified as results of their existence. Secondly, a diagnostic measure given by $\zeta(\nu - 1)$ emerges for a second unstable mode related to the flow-coupled polarity vector instability. This inherent instability is completely suppressed if $\zeta(\nu - 1) > 0$. It can emerge as an additional unstable mode only when $\zeta(\nu - 1) < 0$ and in certain ranges of K and δ . Both the Frank elastic constant and the boundary anchoring condition can expand the region of stability in the phase space (ζ, ν) . On top of it, the active viscosity can induce additional unstable mode provided $\nu < 1$. So, for a flow-aligning rod ACL system, the active viscosity does not introduce any instabilities. It only does so when $\nu < 1$. In this case, it can be stabilizing and destabilizing depending on the active parameter ζ and the geometric parameter ν .

At sufficiently strong bulk activity parameterized by $\zeta < 0$, the unstable Rayleigh mode can be completely suppressed leading to a stable active liquid crystal jets! The condition for attaining a completely stable ALC jet depends on the geometry of the ALC molecules, the activity parameter ζ , active viscosity β , and long range elastic interaction parameterized by the Frank elastic constant. There are parameter regimes where each of the three unstable modes can survive individually, in various combinations or suppressed completely. These rich dynamics of ALC jets can provide various mechanisms for processing free surface active liquid crystal flows. For instance, the modified Rayleigh instability may lead to a change of drop shape as the molecular activities are either extensile or contractile in comparison with the drop formation in a passive or an isotropic fluid. By tuning the ALC material property to completely stabilize the jet flow may enhance formation of long fibers which may has a direct application in regenerative medicine in neural science and organ fabrication. By fine-tuning the three types instabilities, we may be able to select the droplet size and shapes. The exotic behavior in jet instability for active liquid crystals needs to be verified experimentally. Nonetheless, the current theoretical study certainly sheds light on this class of fascinating active matter system and in the meantime poses questions about the validity of the active viscous stress as well.

Acknowledgements

Qi Wang would like to thank AFOSR, NIH and NSF for their financial support through awards FA9550-12-1-0178, DMS-1200487, and 2R01GM078994-05A1.

5 Appendix: Derivation of A Slender Jet Model and Its Dispersion Relation

In long-wave approximations, the length scale in the r -direction is much smaller than in the z -direction. At the leading order, the velocity perturbation is approximately given by $\delta\mathbf{v}(r, z, t) = (r\delta v_r(z, t), 0, \delta v_z(z, t))$, the free surface by $\phi = 1 + \delta\phi$ and the polarity vector $\mathbf{p} = (0, 0, 1 + \delta p_z)$. It follows from the incompressible condition $\frac{\partial v_z}{\partial z} + \frac{1}{r} \frac{\partial(rv_r)}{\partial r} = 0$ that

$$\frac{\partial \delta v_z}{\partial z} + 2r\delta v_r = 0. \quad (5.1)$$

Using the kinematic boundary condition (2.7), we obtain the first order equation

$$\frac{\partial \delta v_z}{\partial z} = -2 \frac{\partial \delta \phi}{\partial t}. \quad (5.2)$$

Next, we use $\mathbf{p} = (0, 0, 1 + \delta p_z)$ and the molecular field $h_r = 0, h_\theta = 0, h_z = -2h_2 \delta p_z + K \frac{\partial^2 \delta p_z}{\partial z^2}$ to obtain the transport equation of \mathbf{p} at this order,

$$\frac{\partial \delta p_z}{\partial t} = \frac{h_z}{\gamma} + \nu \frac{\partial \delta v_z}{\partial z}. \quad (5.3)$$

We rewrite $\boldsymbol{\sigma} = \boldsymbol{\sigma}^t - \Pi \mathbf{I}$, where $\boldsymbol{\sigma}^t$ is the extra stress tensor, the second dynamic boundary condition (2.5) is given by

$$[(\Pi - \Pi_a) \mathbf{I} - \boldsymbol{\sigma}^t] \cdot \mathbf{n} \cdot \mathbf{n} = \tau \left(\frac{1}{R_{rz}} + \frac{1}{R_{r\theta}} \right). \quad (5.4)$$

So, the capillary pressure Π_τ becomes

$$\Pi_\tau = \tau - \tau \left(\delta \phi + \frac{\partial^2 \delta \phi}{\partial z^2} \right), \quad (5.5)$$

where we approximate

$$R_{r\theta} = \sqrt{1 + r'^2} r \approx r = 1 + \delta \phi, \quad R_{rz} = \frac{(1+r'^2)^{3/2}}{-r''} \approx \frac{-1}{\delta \phi''}. \quad (5.6)$$

The pressure Π can be expressed in terms of the capillary pressure [42, 66]

$$\Pi = -\frac{1}{3}(\sigma_{zz}^* + \sigma_{rr}^* + \sigma_{\theta\theta}^*) = -\frac{1}{3}(\sigma_{zz}^* - 2\Pi_\tau), \quad (5.7)$$

where we use the boundary conditions [66]:

$$\sigma_{rr}^* = -\Pi_\tau, \sigma_{\theta\theta}^* = \sigma_{rr}^* \text{ at } r = R = 1, \quad (5.8)$$

and

$$\sigma_{zz}^* = -\Pi + 2\eta \frac{\partial \delta v_z}{\partial z}. \quad (5.9)$$

Then $\Pi = \Pi_\tau - \eta \frac{\partial \delta v_z}{\partial z}$. The only nonzero component of total stress tensor $\boldsymbol{\sigma}$ is [66]

$$\sigma_{zz} = -\Pi_\tau + 3\eta \frac{\partial \delta v_z}{\partial z} - \nu p_z h_z. \quad (5.10)$$

The axial momentum balance equation becomes

$$\frac{\partial \delta v_z}{\partial t} = \frac{\partial \sigma_{zz}}{\partial z}. \quad (5.11)$$

From equations (5.2) and (5.11), we obtain

$$\frac{\partial^2 \delta\phi}{\partial t^2} = -\tau \frac{\partial^2}{\partial z^2} \left(\delta\phi + \frac{\partial^2 \delta\phi}{\partial z^2} \right) + 3\eta \frac{\partial^3 \delta\phi}{\partial t \partial z^2} + \frac{\nu}{2} \frac{\partial^2}{\partial z^2} (p_z h_z). \quad (5.12)$$

After introducing the normal mode

$$\delta\phi(z, t) = \varepsilon e^{\alpha t + ikz} \phi_0, \quad \delta p_z(z, t) = \varepsilon e^{\alpha t + ikz} p_0, \quad (5.13)$$

and substituting them into equation (5.12), we obtain

$$\alpha^2 \phi_0 = \tau k^2 (1 - k^2) \phi_0 - 3\eta k^2 \alpha \phi_0 + \frac{\nu}{2} k^2 (2h_2 + Kk^2) p_0. \quad (5.14)$$

Solving the p_z equation (5.3) for steady states: $\frac{h_z}{\gamma} + \nu \frac{\partial \delta v_z}{\partial z} = 0$, we obtain $(2h_2 + K_1 k^2) p_0 = -2\gamma \nu \alpha \phi_0$. Substituting this into (5.14), we have the dispersion equation for the approximate model

$$\alpha^2 + (3\eta + \gamma \nu^2) k^2 \alpha - \frac{\tau}{2} k^2 (1 - k^2) = 0. \quad (5.15)$$

References

- [1] John Toner and Yuhai Tu. Long-range order in a two-dimensional dynamical XY model: How birds fly together. *Phys. Rev. Lett.*, 75:4326–4329, 1995.
- [2] John Toner and Yuhai Tu. Flocks, herds, and schools: A quantitative theory of flocking. *Phys. Rev. E*, 58:4828–4858, 1998.
- [3] S. Ramaswamy, R.A. Simha, and J. Toner. Active nematics on a substrate: giant number fluctuations and long-time tails. *Europhys. Lett*, 62(2):196–202, 2003.
- [4] V. Narayan, S. Ramaswamy, and N. Menon. Long-lived giant number fluctuations in a swarming granular nematic. *Science*, 317:105–108, 2007.
- [5] A. J. Koch and H. Meinhardt. Biological pattern formation: from basic mechanisms to complex structures. *Rev. Mod. Phys.*, 66:1481–1507, 1994.
- [6] E.O. Budrene and H.C. Berg. Complex patterns formed by motile cells of escherichia coli. *Nature*, 349:630–633, 1991.
- [7] E.O. Budrene and H.C. Berg. Dynamics of formation of symmetrical patterns by chemotactic bacteria. *Nature*, 376(6535):49–53, 1995.
- [8] Tanniemola B. Liverpool. Anomalous fluctuations of active polar filaments. *Phys. Rev. E*, 67:031909, 2003.
- [9] M. Matsushita. *Bacteria as Multicellular Organisms*, chapter 13, page 366. Oxford University Press, New York, Oxford, 1997.
- [10] D. Murray James. *An Introduction To Mathematical Biology*. Springer-Verlag, New York, 3 edition, 2002.

- [11] R. Kline Timothy, F. Paxton Walter, E. Mallouk Thomas, and Angew Ayusman Sen. Catalytic nanomotors: Remote-controlled autonomous movement of striped metallic nanorods. *Chem. Int. Ed.*, 117:754–756, 2005.
- [12] Christopher Dombrowski, Luis Cisneros, Sunita Chatkaew, Raymond E. Goldstein, and John O. Kessler. Self-concentration and large-scale coherence in bacterial dynamics. *Phys. Rev. Lett.*, 93:098103, 2004.
- [13] K. Kruse, J.F. Joanny, F. Jülicher, J. Prost, and K. Sekimoto. Asters, vortices, and rotating spirals in active gels of polar filaments. *Phys. Rev. Lett.*, 92:078101, 2004.
- [14] K. Kruse, J.F. Joanny, F. Jülicher, J. Prost, and K. Sekimoto. Generic theory of active polar gels: a paradigm for cytoskeletal dynamics. *Eur. Phys. J. E*, 16:516, 2005.
- [15] J.F. Joanny, F. Jülicher, K. Kruse, and J. Prost. Hydrodynamic theory for multi-component active polar gels. *New Journal of Physics*, 9:422, 2007.
- [16] Q. Wang, X. Yang, Adalsteinsson David, T. Elston, K. Jacobson, Maryna Maria, and M. G. Forest. *Computational and Modeling Strategies for Cell Motility: Bacteria as Multicellular Organisms*, pages 257–296. Springer, New York, 2012.
- [17] S. Ramaswamy. The mechanics and statistics of active matter. *Annu. Rev. Condens. Matter Phys.*, 1:323, 2010.
- [18] M.C. Marchetti, J.F. Joanny, S. Ramaswamy, T.B. Liverpool, J. Prost, Madan Rao, and R. Aditi Simha. Hydrodynamics of soft active matter. *Rev. Mod. Phys.*, 85:1143, 2013.
- [19] Simha R. Aditi and Sriram Ramaswamy. Hydrodynamic fluctuations and instabilities in ordered suspensions of self-propelled particles. *Phys. Rev. Lett.*, 89:058101, 2002.
- [20] P. G. De-Gennes and J. Prost. *The Physics of Liquid Crystals*. Oxford Science Publications, Oxford, 1993.
- [21] H. Gruler, U. Dewald, and M. Eberhardt. Nematic liquid crystals formed by living amoeboid cells. *Eur. Phys. J. B*, 11:187–192, 1999.
- [22] R. Kemkemer, D. Kling, D. Kaufmann, and H. Gruler. Elastic properties of nematoid arrangements formed by amoeboid cells. *Eur. Phys. J. E*, 1:215–225, 2000.
- [23] Tamás Vicsek, András Czirók, Eshel Ben-Jacob, Inon Cohen, and Ofer Shochet. Novel type of phase transition in a system of self-driven particles. *Phys. Rev. Lett.*, 75:1226–1229, Aug 1995.
- [24] A. Baskaran and M.C. Marchetti. Self-regulation in self-propelled nematic fluids. *Eur. Phys. J. E*, 35:95, 2012.
- [25] David Saintillan and Michael J. Shelley. Instabilities and pattern formation in active particle suspensions: Kinetic theory and continuum simulations. *Phys. Rev. Lett.*, 100:178103, Apr 2008.

- [26] T. B. Liverpool and M. C. Marchetti. Rheology of active filament solutions. *Phys. Rev. Lett.*, 97:268101, Dec 2006.
- [27] A. Baskaran and M.C. Marchetti. Enhanced diffusion and ordering of self-propelled rods. *Phys. Rev. Lett.*, 101:268101, 2008.
- [28] A. Baskaran and M.C. Marchetti. Statistical mechanics and hydrodynamics of bacterial suspensions. *Proc. Natl. Acad. Sci. U.S.A.*, 106:15567, 2009.
- [29] L. Petitjean, M. Reffay, E. Grasland-Mongrain, M. Poujade, B. Ladoux, A. Buguin, and P. Silberzan. Velocity fields in a collectively migrating epithelium. *Biophys. J.*, 98:1790–1850, 2010.
- [30] F. Peruani, J. Starruss, V. Jakovljevic, L. Sogaard Anderseng, A. Deutsch, and M. Bär. Collective motion and nonequilibrium cluster formation in colonies of gliding bacteria. *Phys. Rev. Lett.*, 108:098102.
- [31] Shradha Mishra, Aparna Baskaran, and M. Cristina Marchetti. Fluctuations and pattern formation in self-propelled particles. *Phys. Rev. E*, 81:061916, Jun 2010.
- [32] R. Voituriez, J.F. Joanny, and J. Prost. Spontaneous flow transition in active polar gels. *Europhys. Lett.*, 70:404, 2005.
- [33] David Saintillan and Michael J. Shelley. Orientational order and instabilities in suspensions of self-locomoting rods. *Phys. Rev. Lett.*, 99:058102, 2007.
- [34] David Saintillan and Michael J. Shelley. Instabilities, pattern formation, and mixing in active suspensions. *Phys. Fluids*, 20:123304, 2008.
- [35] Christel Hohenegger and Michael J. Shelley. Stability of active suspensions. *Phys. Rev. E*, 81:046311, Apr 2010.
- [36] Aparna Baskaran and M. Cristina Marchetti. Nonequilibrium statistical mechanics of self-propelled hard rods. *J. Stat. Mech.*, 2010:04019, April 2010.
- [37] T. B. Liverpool, M. C. Marchetti, J. F. Joanny, and J. Prost. Mechanical response of active gels. *Europhysics Letters*, 85(1):18007, 2010.
- [38] A. Gopinath, M.F. Hagan, M.C. Marchetti, and A. Baskaran. Dynamical self-regulation in self-propelled particle flows. *Phys. Rev. E*, 85(6):061903, 2012.
- [39] M. G. Forest, R. Zhou, and Q. Wang. A kinetic theory and its predictions for semidilute active nematic suspensions. *Soft Matter*, 21:5207–5222, 9 2013.
- [40] A. Baskaran and M.C. Marchetti. Hydrodynamics of self-propelled hard rods. *Phys. Rev. E*, 77:011920, 2008.
- [41] D. Rey Alejandro. Capillary models for liquid crystal fibers, membranes, films, and drops. *Soft Matter*, 3:1934, 2007.

- [42] Cheong Ae-Gyeong and D. Rey Alejandro. Capillary instabilities in thin nematic liquid crystalline fibers. *Phys. Rev. E*, 64:041701, 2001.
- [43] S. Bois Justin, Jülicher Frank, and W. Grill Stephan. Pattern formation in active fluids. *Phys. Rev. Lett.*, 106:028103, 2011.
- [44] Giomi Luca and M. Cristina Marchetti. Polar patterns in active fluids. *Soft Matter*, 8:129, 2012.
- [45] Qi Wang. Special cylindrical free surface jets of liquid crystalline polymers and their stability. *Journal of Non-Newtonian Fluid Mechanics*, 90:25–45, 2000.
- [46] Qi Wang. The role of surface elasticity in capillary instability of cylindrical jets of liquid crystalline polymers. *Journal of Non-Newtonian Fluid Mechanics*, 100:97–114, 2001.
- [47] D. Rey Alejandro. Thermodynamic stability analysis of liquid-crystalline polymer fibers. *American Chemical Society*, 36:1114–1121, 1997.
- [48] D. Rey Alejandro. Linear stability theory of break-up dynamics of nematic liquid crystalline fibers. *Journal de Physique II*, 7:1001–1010, 1997.
- [49] Ae-Gyeong Cheong and D. Rey Alejandro. Cahn-hoffman capillarity vector thermodynamics for curved liquid crystal interfaces with applications to fiber instabilities. *Journal of Chemical Physics*, 117:10, 2002.
- [50] Leonid G. Fel and Yoram Zimmels. Rayleigh instability in liquid-crystal jets. *Journal of Experimental and Theoretical Physics*, 98:960–973, May 2004.
- [51] Alexander Zumdieck, Marco Cosentino Lagomarsino, Catalin Tanase, Karsten Kruse, Bela Mulder, Marileen Dogterom, and Frank Jülicher. Continuum description of the cytoskeleton: Ring formation in the cell cortex. *Phys. Rev. Lett.*, 95:258103, Dec 2005.
- [52] A. Zumdieck, R. Voituriez, J. Prost, and J. F. Joanny. Spontaneous flow of active polar gels in undulated channels. *Faraday Discuss.*, 139:369–375, 2008.
- [53] M. E. Cates, S. M. Fielding, D. Marenduzzo, E. Orlandini, and J. M. Yeomans. Shearing active gels close to the isotropic-nematic transition. *Phys. Rev. Lett.*, 101:068102, Aug 2008.
- [54] D. Marenduzzo, E. Orlandini, M. E. Cates, and J. M. Yeomans. Steady-state hydrodynamic instabilities of active liquid crystals: Hybrid lattice boltzmann simulations. *Phys. Rev. E*, 76:031921, Sep 2007.
- [55] D. Marenduzzo, E. Orlandini, and J. M. Yeomans. Hydrodynamics and rheology of active liquid crystals: A numerical investigation. *Phys. Rev. Lett.*, 98:118102, Mar 2007.
- [56] D. Marenduzzo, E. Orlandini, M.E. Cates, and J.M. Yeomans. Lattice boltzmann simulations of spontaneous flow in active liquid crystals: The role of boundary conditions. *J. Non-Newtonian Fluid Mech.*, 149:56–62, 2008.

- [57] Hatwalne Yashodhan, Ramaswamy Sriram, Madan Rao, and R. Aditi Simha. Rheology of active-particle suspensions. *Phys. Rev. Lett.*, 92:11, 2004.
- [58] Giomi Luca, Tanniemola B. Liverpool, and M. Cristina Marchetti. Sheared active fluids: Thickening, thinning, and vanishing viscosity. *Phys. Rev. E*, 81:051908, 2010.
- [59] Qi Wang. A hydrodynamic theory for solutions of nonhomogeneous nematic liquid crystalline polymers of different configurations. *The Journal of Chemical Physics*, 116:9120, 2002.
- [60] S. Fürthauer, M. Neef, S. W. Grill, K. Kruse, and F. Jülicher. The taylor-couette motor: spontaneous flows of active polar fluids between two coaxial cylinders. *New Journal of Physics*, 14:023001, 2012.
- [61] F. M. Leslie. *Theory of flow phenomena in liquid crystals*. Academic Press, New York, 1979.
- [62] J. Elgeti, M.E. Cates, and D. Marenduzzo. Defect hydrodynamics in 2d polar active fluids. *Soft Matter*, 7:3177, 2011.
- [63] Luca Giomi, M. Cristina Marchetti, and Tanniemola B. Liverpool. Complex spontaneous flows and concentration banding in active polar films. *Phys. Rev. Lett.*, 101:198101, 2008.
- [64] S. Chandrasekhar. *Hydrodynamic and Hydromagnetic Stability*. Dover Publications, New York, 1961.
- [65] J. Wang, D. D. Joseph, and T. Funada. Viscous contributions to the pressure for potential flow analysis of capillary instability of two viscous fluids. *Physics of Fluids*, 17:052105, 2005.
- [66] V. G. Levich. *Physicochemical Hydrodynamics*. Prentice-Hall, Englewood Cliffs, NJ, 1962.